Volcanoes Along Convergent Plate Boundaries

12

12.1 Introduction

This chapter focuses on the tectono-magmatic relationships along convergent plate boundaries characterized by subduction: these boundaries are the sites of the largest earthquakes and eruptions and constitute the most active, unstable and hazardous areas on Earth. Volcanic arcs are the surface manifestation of the magmatic activity resulting from plate convergence. As anticipated in Chap. 10, their structural setting may vary significantly, mainly depending on the velocity and angle of convergence between the subducting and overriding plates. The arc may in fact be controlled by predominant extensional, strike-slip, contractional, transtensive or transpressive structures, or any combination of these, with transient kinematic variations induced by mega-earthquakes along the plate boundary. As a result of these variable tectonic and structural features, the distribution and composition of the volcanoes, and their erupted styles, volumes and frequencies may also vary. While a volcanic arc usually consists of a focused belt of andesite stratovolcanoes with subordinate calderas, under specific conditions rhyolitic calderas may predominate, fuelling a much more voluminous explosive activity associated with widespread transcrustal magmatism.

The main aims of this chapter are to:

- describe the tectonic and magmatic features of representative volcanic arcs experiencing predominant extensional, contractional and strike-slip kinematics;
- highlight similarities and differences in the magmatic activity of the arcs as a function of their tectonic context, including any transient variation induced by mega-earthquakes;
- discuss the general role of magmatic activity in the evolution of convergent plate boundaries.

12.2 Extensional Arcs

Extensional arcs are characterized by dominant arc-perpendicular extension. As anticipated in Sect. 10.4, extension may result from a weak coupling between the two converging plates, where the downgoing plate does not push tightly against the overriding plate, with the latter experiencing local extension in its frontal portion. In addition, arc extension may be the local expression of a wider area of back-arc opening, resulting from the different convergence rate between the frontal and inner portions of the overriding plate, under the roll-back of the negatively buoyant slab.

V. Acocella, *Volcano-Tectonic Processes*, Advances in Volcanology,
https://doi.org/10.1007/978-3-030-65968-4_12

Table 12.1 Tectono-magmatic features of active volcanic arcs

ARC	R	EC	SS	Q	V_n	V_p	Q_c
Kamchatka	$3 \pm 0.9 \times 10^{-3}$	10 ± 5	5 ± 3	0.67 ± 0.2	74	13	0.85 ± 0.03
Alaska[pa]	$2.6 \pm 0.5 \times 10^{-4}$	-1 ± 1	0 ± 1	-1 ± 0.5	58	6	0.91 ± 0.04
Cascades	$9.5 \pm 0.4 \times 10^{-4}$	2 ± 1	0 ± 1	1 ± 0.5	24	18	0.57 ± 0.05
North Kuril	$3.6 \pm 1 \times 10^{-4}$	-1 ± 1	0.5 ± 0.5	-0.67 ± 0.2	77	12	0.86 ± 0.03
South Kuril	$3.6 \pm 1 \times 10^{-4}$	-3 ± 2	2 ± 2	-0.6 ± 0.2	71	39	0.64 ± 0.02
Less. Antilles[pb]	$4 \pm 0.6 \times 10^{-4}$	4 ± 1 (ap)	3 ± 2	0.57 ± 0.2	12	3	0.8 ± 0.16
Marianas	$1.25 \pm 0.5 \times 10^{-3}$	5 ± 5	0 ± 1	1 ± 0.5	31	21	0.6 ± 0.04
Central Mexico	$1.37 \pm 0.4 \times 10^{-4}$	0.4 ± 0.04	0.14 ± 0.01	0.74 ± 0.3	51	10	0.84 ± 0.04
Central America[c]	$3.1 \pm 0.8 \times 10^{-3}$	12 ± 2 (ap)	11 ± 2	0.52 ± 0.1	73	6	0.92 ± 0.03
NE Japan[d]	$1.5 \pm 0.4 \times 10^{-4}$	-5 ± 3	0 ± 1	-1 ± 0.5	96	32	0.75 ± 0.02
New Zealand[e]	$2 \pm 0.4 \times 10^{-3}$	6.5 ± 0.2	2.6 ± 0.2	0.71 ± 0.2	41	16	0.72 ± 0.04
Izu-Bonin	$4 \pm 0.9 \times 10^{-4}$	1.7 ± 0.3	0.5 ± 0.5	0.77 ± 0.3	55	20	0.73 ± 0.03
Sumatra[pf]	$6.6 \pm 2 \times 10^{-3}$	0 ± 2	23 ± 2	0	41	18	0.69 ± 0.04
East Aleutians	$2 \pm 0.7 \times 10^{-4}$	-5 ± 5	0 ± 1	-1 ± 0.5	65	14	0.82 ± 0.03
South Andes[g]	$1.3 \pm 0.4 \times 10^{-3}$	-1 ± 1	10 ± 8	-0.09 ± 0	75	27	0.73 ± 0.02
SW Japan[ph]	$3 \pm 0.7 \times 10^{-3}$	4 ± 2(ap)	4 ± 2	0.5 ± 0.1	48	23	0.68 ± 0.03

R = volume of erupted magma (km^3) per year per 100 km of length of the arc; *EC* = amount of arc-normal extension (*E*, positive) or compression (*C*, negative), in mm/year; *SS* = amount of arc-parallel slip (mm/year); arc motion $Q = EC/(|EC| + SS)$; V_n = trench-normal component of the convergence vector V_{con} (mm/year); V_p = trench-parallel component of the convergence vector (mm/year); convergence motion $Q_c = V_n/(V_n + V_p)$. Mean errors associated with V_n and V_p are of ±2 mm/year; p = portion of arc; ap = arc-parallel extension; a = Katmai Province; b = central portion; c = South Guatemala and El Salvador; d = northeast Honshu; e = Taupo Volcanic Zone, North Island; f = Toba region; g = Puyehue-Cordón Caulle region; h = Kyushu region (modified after Acocella and Funiciello 2010)

Several magmatic arcs experience predominant extension, including those in Kamchatka (Russia), Cascades (western North America), Marianas, Izu-Bonin (western Pacific), New Zealand and Central Italy (Table 12.1; Acocella and Funiciello 2010, and references therein). The three representative cases described below consider different conditions of extension. These are exemplified by a volcanic arc with low extension rate, such as the Cascade Arc (Sect. 12.2.1), an arc with high extension rate, as the Taupo Volcanic Zone of New Zealand (Sect. 12.2.2) and an arc developed on the margin of an extended back-arc zone, as the Tyrrhenian margin of Central Italy (Sect. 12.2.3).

12.2.1 Cascade Arc

The Cascade Arc strikes north–south for approximately 1200 km from British Columbia (western Canada) to Northern California (western USA). The arc lies above a warm slab convergence zone, where the young (less than 10 Ma) oceanic crust of the Juan de Fuca plate subducts beneath the North American plate north of the Mendocino Triple Junction. At this junction, the tectonic environment shifts from northwest directed shear along the San Andreas Fault to E-W trending convergence along the Juan de Fuca plate (Fig. 12.1; Hildreth 2007 and references therein). Beneath the Cascade Range,

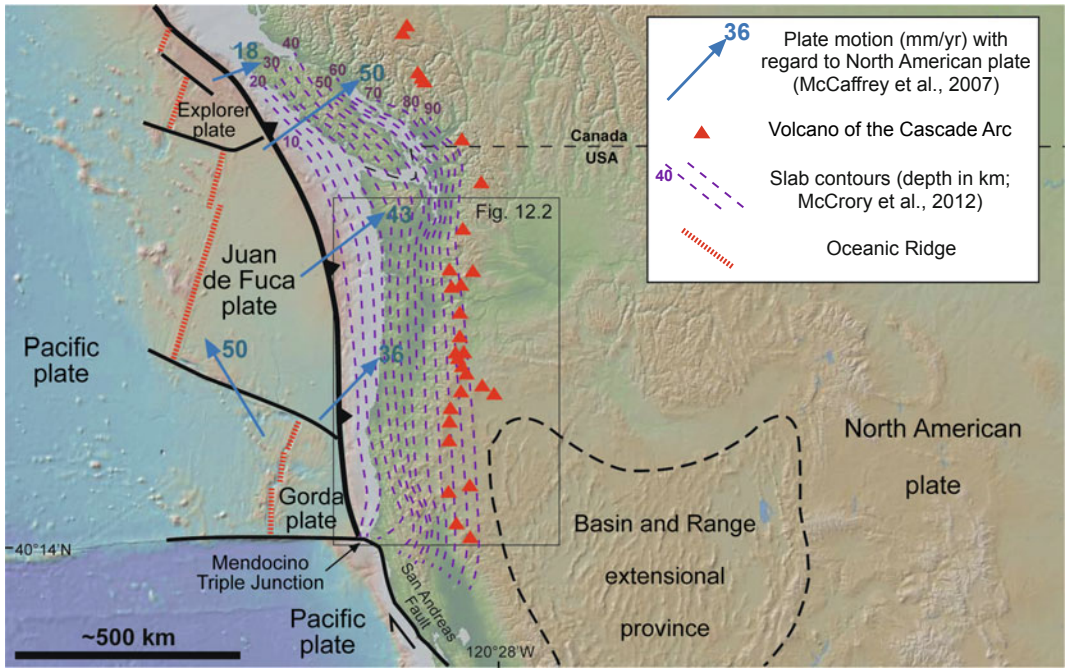

Fig. 12.1 Tectonic setting of the Cascade Volcanic Arc, western North America, showing the major plate boundaries, the slab contours and the vectors of plate motion (modified after McCaffrey et al. 2007). Base DEM provided by GeoMapApp

the Juan de Fuca slab is seismically imaged as a high velocity zone dipping 65°, extending at least to 200 km of depth. This convergence zone is one of the best-documented subduction systems for episodic tremor and slow-slip earthquakes. The crust beneath the Cascades of Oregon is 40 km thick, thinning to 31 km eastward; the 42–47 km thicker crust beneath the Washington Cascades, to the north, may result from underplating. The magmatically most active Oregon portion of the arc shows low seismic velocities at all depths, suggesting widespread melt. The less active Washington portion shows high seismic velocities in the upper mantle and upper crust, possibly due to solidified intrusions. More localized and shallower low velocity zones supportive of ~6% of melt have been imaged below the volcanoes of Mount St. Helens, Mount Adams and Mount Rainier, in the southern Washington Cascades: these are indicative of large-scale basaltic sill emplacement and silicic differentiation, representing the primary reservoir of the region's arc magmatism (Miller et al. 1997; Parsons et al. 1998; Pollitz et al. 2010; Gao et al. 2011; Flinders and Shen 2017).

Northeast-directed subduction of the Juan de Fuca plate results in nearly arc-normal convergence in the northernmost portion of the Cascade Arc, but oblique convergence elsewhere. This imparts a dextral component in the forearc region, from central Washington to California (Hildreth 2007, and references therein). In particular, in the northern Cascades the direction of the maximum principal stress σ_1 changes from margin-normal along the coast to margin-parallel inland. While the former is related to the coupled interface between the North America and Juan de Fuca plates, the latter derives from the motion of the Juan de Fuca plate, which ultimately results in a northward movement at a few mm/yr of the forearc. The Cascades also rotate clockwise with regard to North America at a rate of 0.4–1°/Ma (Fig. 12.2). A southward increase in rotation parallels a change in the arc tectonic regime, from largely contractional in northern Washington to extensional in Oregon. Concomitant is a

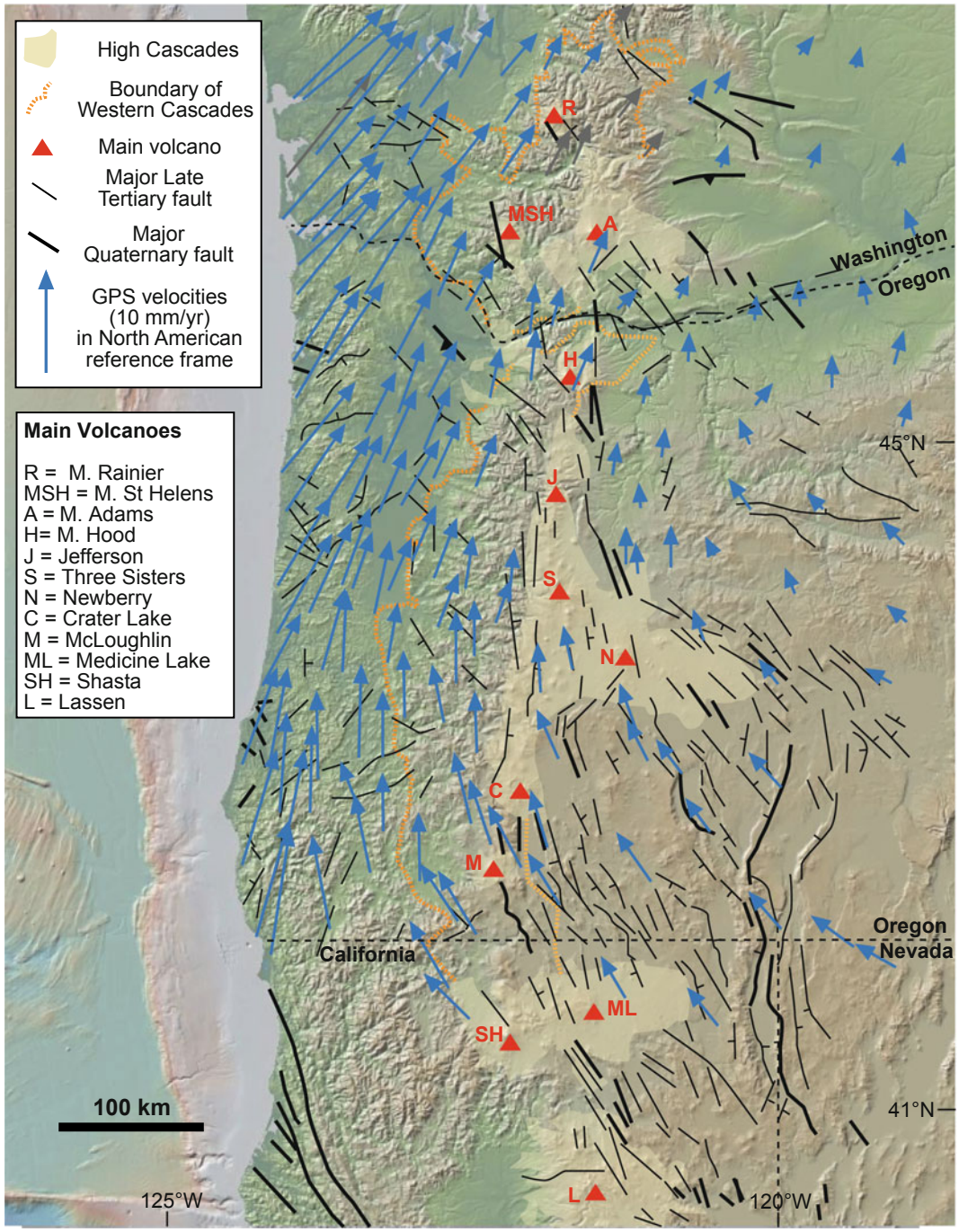

Fig. 12.2 Geology (extent of the Western and High Cascades), structure (late Tertiary and Quaternary faults), present kinematics (GPS motions between 1991 and 2004) and volcanism (main volcanoes) along the central and southern portions of the Cascade Volcanic Arc (Pezzopane and Weldon 1993; Blakely et al. 1997; McCaffrey et al. 2007). Base DEM provided by GeoMapApp

southward increase in the volume of eruptive rocks along the volcanic arc. Extension across the southern part of the arc is also promoted by the buoyant mantle beneath the western Basin and Range Province (Wells 1990; Hildreth 2007; McCaffrey et al. 2007; McCrory et al. 2012). As a result, crustal deformation across Oregon indicates motion of 0.6 cm/year in a N60°W direction, resulting from combined horizontal extension and dextral shear. This motion can account from 10 to 20% of the total Pacific–North American transform motion and much of the lateral component of relative motion between the Juan de Fuca and North American plates. However, only a minor portion of this extension, geodetically undetected (~0.1 cm/year), affects the volcanic arc (Fig. 12.1; Blakely et al. 1997; McCaffrey et al. 2007). Active extension is usually associated with ~N-S trending half-grabens with major offset to the west. In the southernmost portion of the Cascade Arc, the active structures shift from ~N-S trending normal faults to ~NW–SE trending dextral transtensive systems reaching the northern Sierra Nevada (Pezzopane and Weldon 1993; Waldien et al. 2019).

Two distinct volcanic assemblages characterize the central Cascades of Oregon: the Western Cascades and the High Cascades (Fig. 12.2). The Western Cascades were active since ~40 Ma, with volcanism younging eastward during Miocene and Pliocene, towards the High Cascades. The High Cascades have been active since 8–10 Ma in a focused area of extension (Wells and McCaffrey 2013). Eruption rate along the Cascade Arc decreased by a factor of 3 from 35 to 7 Ma, probably due to the slowing of the plate convergence rate and the increase in the obliquity of subduction. Eruption rate then increased in the last 7 Ma, likely because of the new extensional regime promoting mafic volcanism: volcanic production seems therefore a function of convergence rate and upper plate stress regime (Priest 1990; Hildreth 2007; Pitcher et al. 2017).

Of the 2339 Quaternary volcanoes identified in the current Cascade Arc, 37 are andesite-dacite stratovolcanoes and major silicic dome complexes, 110 are shield volcanoes, 340 are lava domes and more than 1850 are monogenic vents. The main Cascade stratovolcanoes exhibit spacings that range from 35 to 170 km. The composition of the erupted products ranges widely and continuously, and includes olivine tholeiites, intraplate basalts, calcalkaline basalts, basaltic andesites, potassic shoshonites, andesites, rhyolites, rhyodacites and dacites. Primitive basalts produce scoria cones, small shields and discrete lava fields, but virtually never erupt centrally at stratovolcanoes, where more evolved compositions dominate as a result of large fractionating reservoirs (Hildreth 2007). The different age of the subducted plate also influences the depth of melting in the mantle wedge beneath the arc and the general composition of the magmas. Younger and hotter oceanic crust undergoes dehydration with minor amount of heating during subduction. The slab may lose much of its volatiles trenchward of the arc, with a lower volatile budget beneath the arc. This occurs in the northern Cascades, where the contribution of the slab fluids in driving arc magmatism is limited and alkali basalts are frequent. Conversely, dehydration reactions are delayed in older oceanic lithosphere and a greater amount of volatiles are released beneath the central-southern Cascade Arc; this results in higher degrees of melting, producing calkalkaline basalt magmas (Green and Harry 1999).

The Quaternary Cascade Arc is 25–100 km wide and its continuity is interrupted by several gaps containing few or no volcanoes. Assuming that the slab dehydrates and the wedge convects and melts continuously along the whole subduction margin suggests that sectors experiencing lower crustal extension locally stall and suppress the intrusion of mantle melts, likely explaining the gaps. On the other hand, higher extension promotes the eruption of the mafic melts. The gaps also define several segments (four to six, depending on the studies) with distinct direction, structure, geochemical composition and melting regimes at depth, reflecting differences not only in tectonic setting, but also in subduction geometry and mantle heterogeneity. While the degree of melting and fluxing is greatest in the southernmost segment, enhanced

by a slab window, the central segments show higher and focused extension and heat flow, as well as most of the eruptive vents (Fig. 12.2; Guffanti and Weaver 1988; Pezzopane and Weldon 1993; Hildreth 2007; Schmidt et al. 2008; Pitcher and Kent 2019).

In addition to Mount St. Helens, several volcanoes in the southern part of the arc, including Lassen, Shasta, McLoughlin, seem to lie in localized zones of E-W trending extension controlled by the activity of offset NW–SE trending dextral faults (see also Fig. 6.20a; Weaver et al. 1987; Hildreth 2007). Many volcanoes and volcanic complexes have been recently active in the Cascades. Among these, Lassen Peak (northern California) erupted in 1915, whereas Mount St. Helens (described in Sect. 6.8.2) has been erupting since 1980. In the last decades, deformation studies have identified surface displacements at five of the 13 major Cascade Arc volcanoes (Mount Baker, Mount St. Helens, South Sister, Medicine Lake, and Lassen). No deformation has been detected at five volcanoes (Mount Rainier, Mount Hood, Newberry Volcano, Crater Lake, and Mount Shasta), and there are not sufficient data for a rigorous assessment at the remaining three (Glacier Peak, Mount Adams, and Mount Jefferson; Poland et al. 2017).

12.2.2 Taupo Volcanic Zone of New Zealand

Taupo Volcanic Zone (TVZ) lies in the North Island of New Zealand and is probably the best-known volcanic arc undergoing sustained extension. The NNE-SSW trending TVZ results from convergence between the Australian plate and the westward subducting Pacific plate. The plate interface is offshore and to the east of the North Island of New Zealand, along the Hikurangi Trough (Fig. 12.3; e.g., Stern et al. 2006). The northern offshore continuation of the TVZ arc is the Havre Trough, a young back-arc basin where the original arc occupied a narrow area,

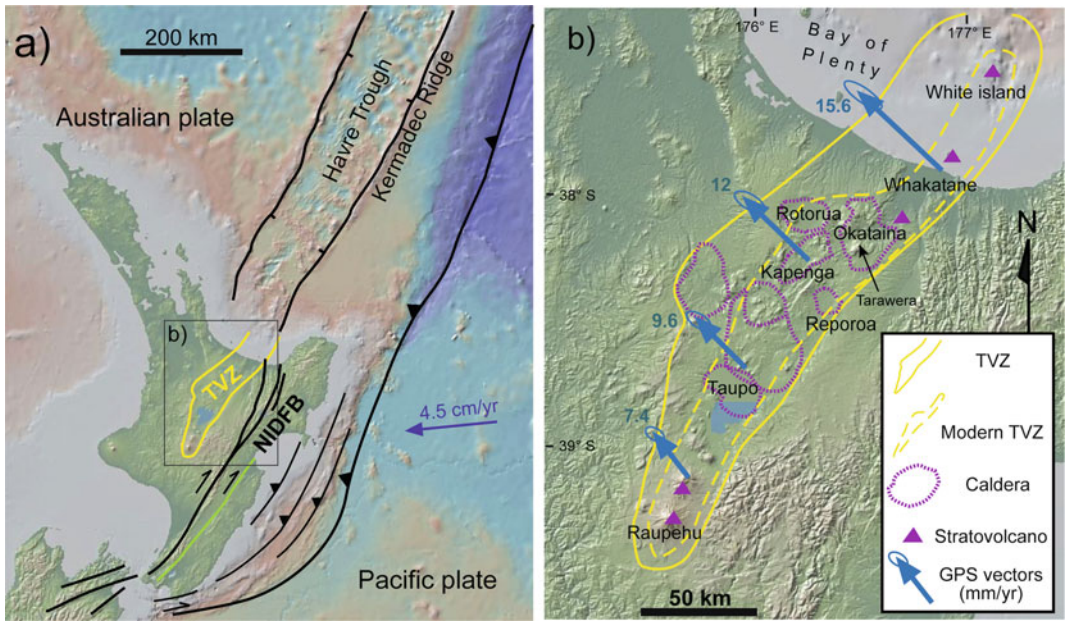

Fig. 12.3 Tectonic setting and main features of Taupo Volcanic Zone (TVZ), New Zealand. **a** Schematic relationship of TVZ to the boundary between the Pacific and Australian plates and fore-arc structures, including the NIDFB (North Island Dextral Fault Belt). **b** Overview of the TVZ, showing the major caldera complexes and stratovolcanoes. Blue arrows show GPS movement of the Australian plate with regard to the fixed Axial Range to the east of TVZ (Wallace et al. 2004). Base DEM provided by GeoMapApp

10–15 km wide, followed by seafloor spreading at ~5.0 Ma, after which arc magmatism dominated again. This rapid sequence of tectono-magmatic regimes is related to the roll-back of the Pacific slab, which may have diverted the arc flux outside the region of seafloor spreading of the back-arc and induced the vertical realignment of surface volcanism with the source of arc melts above the slab (Caratori Tontini et al. 2019). Considered together, the TVZ-Havre Trough system shows an overall northward transition from arc to back-arc magmatism.

At the latitude of TVZ, the mean convergence vector of ~4.5 cm/year between the Australian and Pacific plates is partly oblique, oriented at ~263°. As a result, the area between the trench and the volcanic arc is characterized by an overall constant component of dextral shear, estimated at ~0.25 cm/year. This shear dominates along the North Island Dextral Fault Belt (NIDFB), as the convergence-parallel component passes from dominant contraction in the trench area to negligible contraction along the NIDFB and to dominant extension in the TVZ (Acocella et al. 2003, and references therein).

The current TVZ consists of a rift zone associated with crustal thinning of up to 15 km. Lower crust underplating is significant, with partial melt between 1 and 4%. These features may be related to abundant dehydration fluids coming off the slab at specific locations and migrating upward to the highly fractured volcanic zone. The high mantle flux and rifting are responsible for a remarkably thin (~16 km) and extended crust highly permeable to magma, accounting for the extremely high erupted volumes (Wilson 1996; Bertrand et al. 2012; Gravley et al. 2016; Eberhart-Phillips et al. 2020). Volcanic activity in the last ~2 Ma focused in short periods (25–50 ka) of intense volcanism bracketed by longer periods (100–130 ka) of quiescence, rapidly and asymmetrically narrowing via inward and eastward migration of faulting and also propagating southward. The eastward migration of volcanic activity and faulting followed the roll-back of the Pacific slab at the Hikurangi subduction zone: the correlation in time and space of the loci of voluminous volcanic eruptions and active faulting suggests that a controlling factor in rapid rift narrowing are large shallow crustal heterogeneities, as rhyolitic magma bodies generated by the subduction weakening the crust and localizing deformation (Villamor et al. 2017).

The present site of active volcanism focuses in a NNE-SSW trending narrow zone (20–30 km wide), referred to here as the modern TVZ (Fig. 12.3) and mainly developed in the last ~300 ka, although limited evidence of off-rift magmatism is suggested by seismicity and uplift (Wilson et al. 1995; Hamling et al. 2016). The modern TVZ consists of five main segments displaying an overall graben structure. Each segment shows a variable extension direction, with minor dextral shear resulting from the slightly oblique convergence. GPS measurements and fault slip data suggest a current spreading rate of 0.6–0.8 cm/year across central TVZ, at times with significant transient variations. This extension is associated, in the central portion of TVZ, with overall subsidence of up to 2 cm/year, probably resulting from the cooling and subsequent contraction of shallow magma. This subsidence is confined by a wider zone which coincides with the area of the wider and older TVZ and that is being uplifted of 0.1 cm/year by basaltic melts being injected at depth (Cole 1990; Darby and Meertens 1995; Villamor and Berryman 2001; Hamling et al. 2015; Holden et al. 2015; Houlie and Stern 2017). Seismic activity has been accompanying extension along TVZ, with the most recent significant earthquake (magnitude *M6.5*, in 1987) occurring in the northern part. Shallow microearthquakes may represent up to ~30% of the geodetic deformation, suggesting that the associated small-scale faulting records strains not geologically measured, possibly explaining the disparity between geological and GPS rates of extension across TVZ (Begg and Mouslopoulou 2010; Mouslopoulou et al. 2013).

From a volcanological point of view, the modern TVZ is divided into three parts along its length. (a) The two lateral parts with andesite-dacite stratovolcanoes (Ruapehu-Ngauruhoe-Tongariro volcanoes to the south and

Whakatane-White Island volcanoes to the north). (b) A central part with rhyolitic caldera systems (from Okataina to Taupo calderas) and plutons at depth. This is an extraordinarily productive region of rhyolitic volcanism (~8800 km^3/Ma) and geothermal fluxes (~4200 MW), enhanced by vertical low resistivity zones connecting to magmatic sources below the brittle-ductile transition, at 6–7 km. Here the two largest rhyolitic magmatic systems, Taupo and Okataina, erupted thousands of km^3 of ignimbrites in the last 300 ka. Okataina caldera produced the largest historic eruption, a basaltic Plinian, in TVZ along the NE-SW trending 1886 Tarawera fissure, which is still geodetically extending (Fig. 12.4; Nairn and Cole 1981; Spinks et al. 2005; Holden et al. 2015). Taupo caldera has the capability to generate and erupt very rapidly, within 1–100 years, large crustal melts of ~100 km^3 in volume (Barker et al. 2016). The andesitic-rhyolitic-andesitic composition of TVZ is probably related to different water contents in the lower crust (Heise et al. 2007; Deering et al. 2008). Rhyolites derive from diorites accumulated in the mid crust resulting from the differentiation of hot and water rich basaltic magmas produced in the mantle wedge and intruded as sills within the lower metasedimentary crust.

The relationships between regional tectonic extension and magmatic activity have been repeatedly addressed at TVZ. In the lower crust, fast seismic wave speeds suggest that magma has partially filled the stretched crust, with the extended zone coinciding with an area of intruded magma located between 4 and 15 km depth. This implies a feedback relationship influencing the locations of faults and magma: while extension helps magma to rise, the intruded magma heats and weakens the crust to assist more rifting. At the surface, there is an overall along- and across-strike partitioning of extension and volcanism, with the most productive sectors located along the rift axis, feeding polygenetic calderas controlled by the highest amount of regional extension orthogonal to the rift segment (Fig. 12.5; Acocella et al. 2003; Spinks et al. 2005; Gase et al. 2019). Extension at the surface may result from regional tectonics and/or shallow magmatic processes (i.e., diking). The prevalence of one process or the other within a portion of TVZ mainly depends on the availability of magma. While diking assists extension along the

Fig. 12.4 View of part of the ~NE-SW trending 1886 Tarawera eruptive fissure, on the southern portion of Okataina caldera, Taupo Volcanic Zone

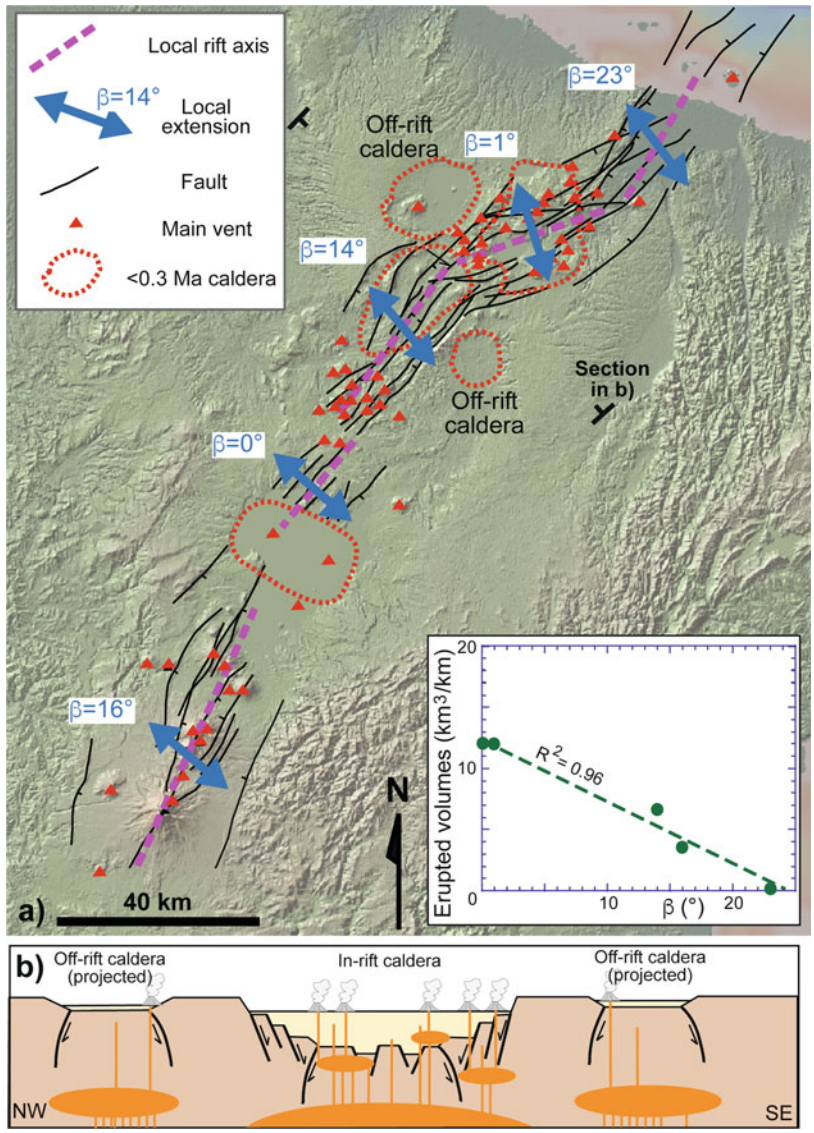

Fig. 12.5 **a** Map of Taupo Volcanic Zone, showing the main volcanoes and the along-rift variations in the dextral component of extension along the rift segments (proportional to the angle β between the opening direction of the rift segment and the perpendicular to the segment strike). The diagram in the inset shows that the magmatically most productive portions undergo orthogonal extension ($\beta \sim 0°$). **b** Across-rift difference in caldera structure: the more productive in-axis polygenetic calderas are deeper and shaped by regional tectonics (see also map view above), whereas off-axis monogenic calderas are less developed and subcircular (Spinks et al. 2005). Base DEM provided by GeoMapApp

most active magmatic portions, regional extension dominates along the magmatically less active portions. For example, field and modelling data across the southern andesitic part of TVZ suggest that the 0.7 cm/year extension is mostly tectonic: here regional faulting accommodates 78–95% of the total extension, while the reminder is accommodated by diking. On the other hand, the 1886 Tarawera event, at Okataina caldera, shows how diking assists extension along the most active magmatic portions. These behaviours imply some complementarity between

regional tectonic faulting and diking, although the two processes may be often coupled. In fact, in some parts of TVZ a correlation between increased slip along regional faults and activity from nearby andesitic volcanoes (Ruapehu) or calderas (Rotorua and Ohakuri) has been recognized (Gravley et al. 2007; Villamor et al. 2007, 2011; Seebeck and Nicol 2009; Rowland et al. 2010; Allan et al. 2012; Gomez-Vasconcelos et al. 2017).

12.2.3 Tyrrhenian Margin of Central Italy

The Tyrrhenian margin of Central Italy hosts a volcanic arc located on the northeastern extended portion, or margin, of the back-arc basin of the Tyrrhenian Sea, characterized by significant crustal thinning and incipient oceanization in the southern part. Extensional processes have been affecting the northeastern Tyrrhenian margin since late Miocene as a consequence of back-arc opening. Extension occurred at the back of the eastward migrating Apennine fold and thrust belt, due to the progressive eastward shift of the Apennine subduction (Fig. 12.6a; Malinverno and Ryan 1986; Royden et al. 1987; Patacca et al. 1990). The eastward migration of subduction, and of the associated extension to its rear, is related to the roll-back of the slab. The active slab is currently limited to the portion of the oceanic Ionian lithosphere subducting below Calabria, with the sides below Sicily and the northern and central Apennines experiencing collision between the African and Eurasian continental plates. The product of this collision-subduction-collision configuration is a convergence front that is strongly arcuate and migrating towards the oceanic subducting lithosphere. As a result of this southeastward migration, the southern Tyrrhenian area has been experiencing larger amounts of back-arc extension (5–6 cm/year), associated with incipient oceanization, with regard to the northern Tyrrhenian area (1–2 cm/year; Patacca et al. 1990; Benoit et al. 2011; Savelli and Ligi 2017). Seismic tomography data show gaps within the previously subducted lithosphere below the Tyrrhenian margin of Central Italy, which are interpreted as deep (100–500 km) subvertical tear faults driving post-collision slab breakoff. These tear faults are inferred to control the presence of magmatic activity along the northeastern Tyrrhenian margin (Wortel and Spakman 2000; Rosenbaum et al. 2008; Giacomuzzi et al. 2012).

In Central Italy, the overall NE-SW directed extension associated with NW–SE trending normal faults has migrated eastward from the Tyrrhenian area during Miocene-Pliocene to the Apennines divide during Quaternary, where extension currently manifests through seismogenic faults. Although geodetic or seismological evidence of active extension has not been detected along the northeastern Tyrrhenian margin, here the minimum horizontal stress is currently mainly NE-SW oriented, and locally NW–SE oriented. Extension has produced a thinner crust ($\sim$25 km) in the eastern side of the Apennines with regard to the western part ($\sim$35 km). Associated with crustal thinning is a high heat flux, which reaches 400 mW m^2 in some volcanic areas along the northeastern Tyrrhenian margin and in the Southern Tyrrhenian area (Jolivet et al. 1998; Serpelloni et al. 2005; Di Stefano et al. 2011; Montone et al. 2012; D'Agostino 2014).

The variable amount of stretching along the northeastern Tyrrhenian margin is highlighted by the different width of the extended area and the morphotectonic variations in the lateral continuity of the extensional basins. In fact, the NW–SE trending normal faults extending the margin formed several Plio-Quaternary basins, partly reactivating pre-existing thrust planes generated during the build up of the Apennines orogen. Transverse NE-SW trending faults often interrupt the continuity of these basins, also forming transverse extensional basins, 1–3 km deep, filled by Plio-Quaternary sedimentary and volcanic deposits. The frequency of the transverse structures decreases northeastward, following more limited extension (Fig. 12.6; Mariani and Prato 1988; Faccenna et al. 1994). Surface and subsurface data show that these orthogonal fault systems crosscut each other, suggesting a coeval

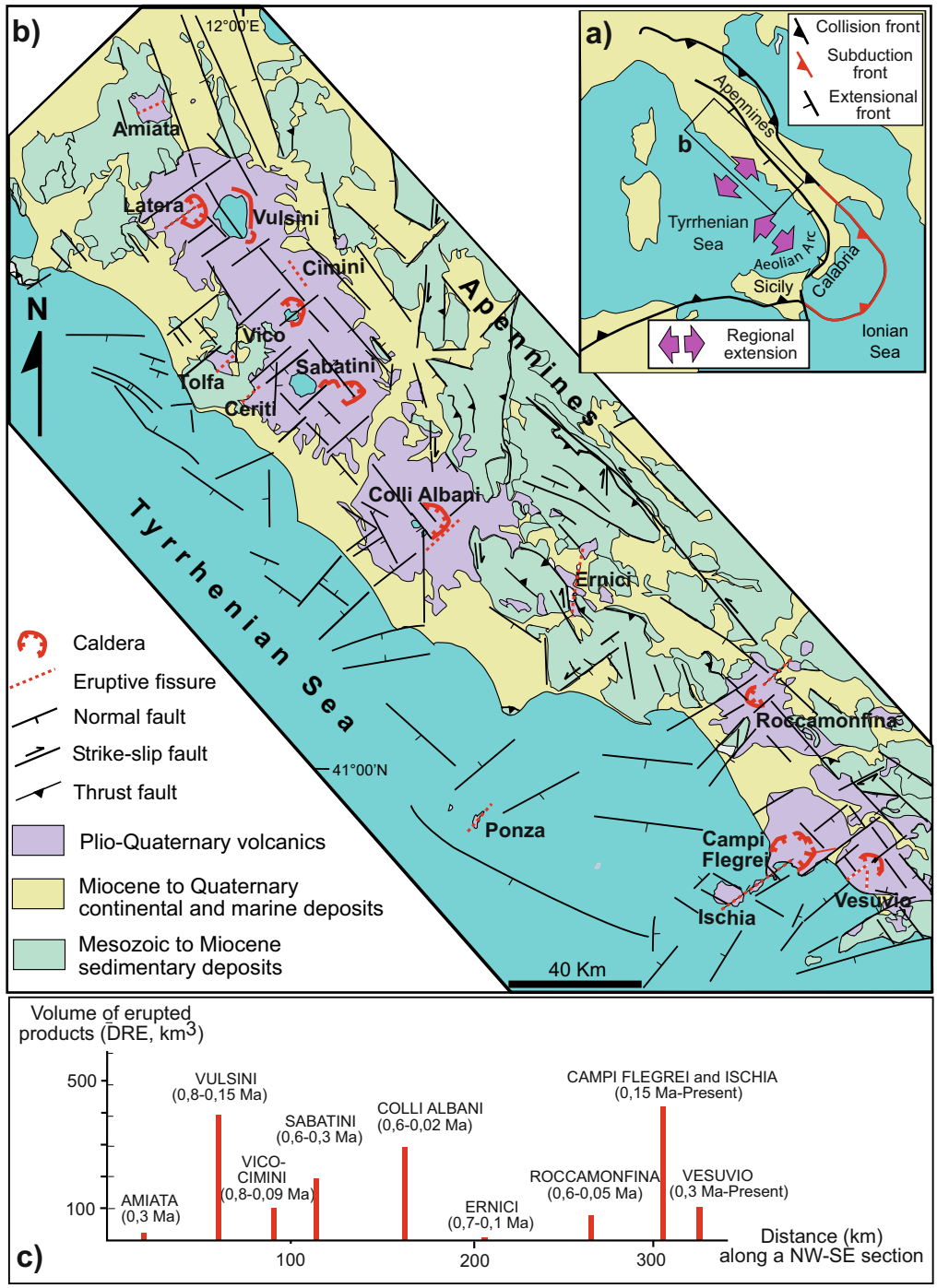

Fig. 12.6 **a** Tectonic setting of the Tyrrhenian margin of Central Italy, showing the orthogonal extension due to the retreat of the Apennines to the northeast (NE–SW extension) and southeast (NW–SE extension) following the arcuate collision-subduction-collision front. **b** Structural setting of the northeastern Tyrrhenian margin, with the main fault systems and the Plio-Quaternary volcanoes. **c** Spacing of volcanoes and related erupted volumes and erupting times (in brackets) projected along a NW–SE trending section (modified after Acocella and Funiciello 2006)

and joint eastward migration. While the margin-parallel faults accommodate crustal extension, the transverse systems may result from two different processes. With predominant transtension, these may be transfer systems of the NW–SE striking normal faults, accommodating the differential extension along the margin. With predominant extension, as in the southern part, these may accommodate the NW–SE oriented extension induced by the retreat of the Ionian slab beneath Calabria, in the southern Tyrrhenian area (Acocella and Funiciello 2006).

Potassic volcanism associated with slab tearing and breakoff beneath the Apennines followed extension along the margin, with compositional signatures transitional between arc type and OIB type magmas. Indeed, the slab breakoff related potassic volcanism of the margin appears distinct from the back-arc basaltic volcanism in the oceanic patches within the Tyrrhenian Sea and from the ongoing calcalkaline volcanism of the Aeolian Arc, which results from the subduction of the Ionian slab (Rosenbaum et al. 2008; Giacomuzzi et al. 2012; Peccerillo 2017). Several volcanic districts are found along the margin: these are NW–SE aligned, parallel to the main normal faults, and have been mostly erupting between ~0.6 and ~0.1 Ma, with the exception of the southernmost area, active from ~0.4 Ma to Present. There is a cyclic behaviour of volcanic activity through the margin, with climax of each major eruptive cycle occurring simultaneously at the different districts every ~48 ka, with most eruptions focusing between 450 and 200 ka (Marra et al. 2004). The northern region, hosting the volcanoes from the Amiata to the Sabatini areas, experienced widespread late Pliocene–Quaternary uplift of a few hundred of metres, probably resulting from repeated magma emplacement (Barberi et al. 1994). The volcanoes mainly consist of caldera complexes with minor relief (Vulsini, Sabatini, Campi Flegrei) or stratovolcanoes with summit calderas (Vico, Colli Albani, Roccamonfina and Vesuvio). Their mean spacing of 42 ± 13 km implies a quite regular distribution. However, this does not correspond to an uniform distribution of the erupted volumes, with most magma being usually erupted at calderas (Vulsini, Sabatini and Campi Flegrei; Fig. 12.6c). In addition, minor volcanic activity occurred from scattered dike-fed monogenic vents between major volcanoes and also within the Central Apennines chain. For example, the emplacement of a dike at ~15 km depth a few tens of kilometres to the east of Roccamonfina volcano in 2013–2014 suggests ongoing magma intrusion also within the mountain chain (Acocella and Funiciello 2006; Peccerillo 2017; Di Luccio et al. 2018). Despite recent minor unrest at Colli Albani, active volcanism focuses to the south, in the Campi Flegrei and Somma-Vesuvio districts. The NE-SW elongated Campi Flegrei District includes the Campi Flegrei Caldera and Procida and Ischia islands, mainly erupting trachytes from ~0.15 Ma to Present. Somma-Vesuvio, active between ~0.3 Ma to Present, mainly erupted phonolites and trachybasalts at the intersection of orthogonal fault systems (Fig. 12.7). Petrological data suggest that, rather than deriving from the extinct subduction below the Central Apennines, these active volcanoes are related to the ongoing subduction of the oceanic Ionian lithosphere below the southern Tyrrhenian area (Rosi and Sbrana 1987; Santacroce 1987; Vezzoli 1988; Passaro et al. 2016; Peccerillo 2017).

Analysis of the fracture systems in the volcanic areas along the margin suggests that the main volcanoes lie at the intersection between the orthogonal fault systems, with the transverse structures predominating over the NW–SE trending structures. This also holds for the major eruptive fissures, which commonly have a transverse direction and moreover erupt the most primitive products (Fig. 12.6). Volcanoes with smaller erupted budget are usually associated with isolated transverse systems (Vico, Vesuvio), whereas volcanoes with higher erupted budget are usually associated with diffuse transverse structures, controlling the shape of calderas and bordering transverse basins usually to the west of the volcano (as at Vulsini, Sabatini, Colli Albani, Campi Flegrei). The onset of sedimentation in these transverse basins is 2–3 Ma older than the

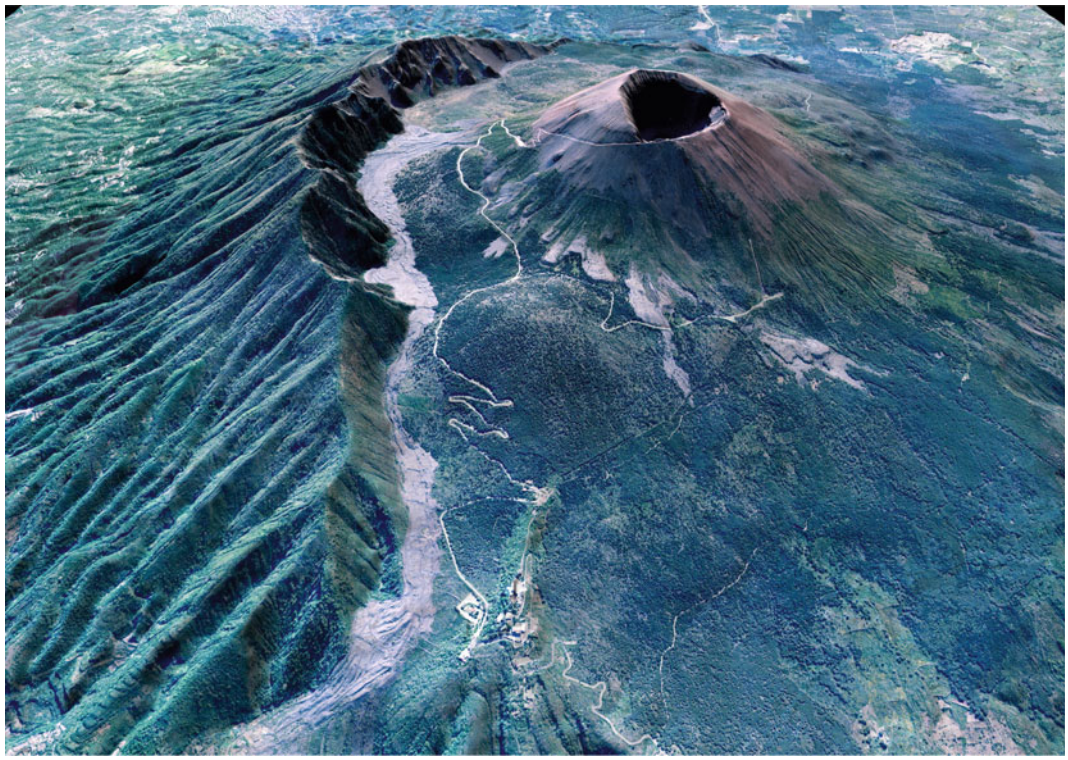

Fig. 12.7 View from the west of the Somma-Vesuvio Volcanic Complex, the last erupting volcano (in 1944) along the Tyrrhenian margin of Central Italy. Mount Somma (to the left) identifies the relict volcano, developed before ~18 ka, separated by the younger arcuate caldera scarp from the active Vesuvio cone (right), developed in the last ~2 ka; the last 1944 lava flow (light colour) lies against part of the caldera scarp. Image courtesy of Giuseppe Vilardo and Laboratorio Geomatica e Cartografia, Osservatorio Vesuviano-INGV

onset of the nearby volcanic activity, suggesting localized pre-volcanic thinning and decompression (e.g., Mariani and Prato 1988; Faccenna et al. 1994).

In synthesis, despite the overall NW–SE orientation of the volcanic arc, there is limited evidence for the activity of NW–SE trending structures controlling magmatism. This is also supported by the fact that active extension due to the NW–SE structures is currently detected within the Apennines ~100 km to the east, and it is likely that such extension already migrated to the east of the volcanic arc during the climax of volcanism between 450 and 200 ka (Devoti et al. 2011; D'Agostino 2014). Therefore, the activity of the NW–SE striking faults along the northeastern Tyrrhenian margin predated volcanic activity, promoting magmatism by thinning the crust and inducing decompression melting. The transverse structures are more closely related to volcanic activity: these may have controlled volcanism in a three-fold way (Fig. 12.8). With a dominant extensional component, as in transverse basins, the transverse structures may localize crustal thinning and decompression, focusing magmatism below the main volcanoes. In addition, any local NW–SE trending extension (especially towards the south) may control dike propagation along a transverse trend. Finally, with a dominant strike-slip component, the transverse structures may provide preferred subvertical crustal paths reactivated by the dikes feeding the major fissure eruptions. The Tyrrhenian case shows how slab breakoff and regional extension promote the overall generation and rise of magma along the margin, but transverse

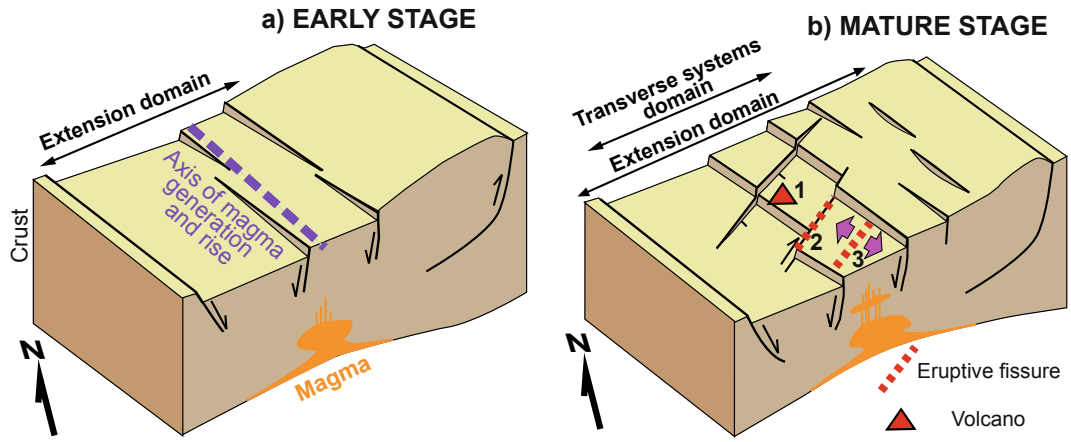

Fig. 12.8 Model of structural control on magmatism along the Tyrrhenian margin of Central Italy. **a** Early stage: extension and decompression due to NW–SE striking normal faults promote magmatism along a NW–SE trending area of partial melting above the torn slab (not shown). **b** Mature stage: extension has migrated to the present Apennines divide. Transverse systems to the back focus the rise of magma in the upper crust, with transverse extensional basins below polygenic volcanoes (1), NE-SW trending dikes intruding subvertical transverse strike-slip faults, (2), or perpendicular to a local NW–SE trending extension, feeding eruptive fissures (3). Not to scale (modified after Acocella and Funiciello 2006)

structures, due to a complex tectonic setting, focus shallower magma rise, emplacement and eruption (Acocella and Funiciello 2006).

12.3 Strike-Slip Arcs

Strike-slip volcanic arcs are characterized by predominant horizontal motion, usually expressed through a principal displacement zone. As described in Sect. 10.4, this condition results from the strain partitioning generated by the oblique convergence between the two plates, with the sense of motion of the trench-parallel component of the convergence vector coinciding with the sense of motion of the strike-slip fault zone along the arc. Strain partitioning, and thus strike-slip arcs, may develop with variable obliquity of the convergence vector: this is expressed by the angle ϕ between the convergence vector and the trench-perpendicular component: the higher the angle, the higher the obliquity (Fig. 10.12). Some strike-slip arcs are related to minor obliquity (of a few tens of degrees), whereas others are related to higher obliquity (several tens of degrees; Table 12.1). While obliquely convergent arcs show a predominant strike-slip motion, a non-negligible contractional or extensional arc-orthogonal component is also commonly found, frequently giving the arc an overall transtensive or transpressive kinematics.

Below two representative cases of strike-slip arcs experiencing minor obliquity (the South Andean Volcanic Zone; Sect. 12.3.1) and major obliquity (Sumatra, Indonesia; Sect. 12.3.2) are described.

12.3.1 The South Andean Volcanic Zone

The N-S trending South Andean Volcanic Zone results from the subduction of the Nazca plate beneath the South American plate in central and southern Chile. To the south of this volcanic zone, after a volcanic gap nearby the Chilean Triple Junction where the spreading Chile Ridge enters the Chile Trench, begins the Austral Volcanic Zone, a young arc related to the Quaternary subduction of the Antarctic plate beneath South America (e.g., Stern 2004).

At the latitude of the South Andean Volcanic Zone, the 0–45 Ma old Nazca plate is being subducted below the continent at 6–9 cm/year in a northeast direction. The dip of the slab increases from ~20° at the northern end of the volcanic zone to >25° further to the south. As a consequence, the distance between the trench and the volcanic arc decreases from more than 290 km in the north to less than 270 km in the south. In addition, the depth to the slab below the arc decreases southwards, from 120 to 90 km (Stern 2004). The convergence between the Nazca and South American plates associated with the South Andean Volcanic Zone is moderately oblique, as the angle between the convergence vector and the trench-perpendicular direction is ~22°. This obliquity is partly partitioned into a contractional forearc and a ~N-S striking domain along the volcanic arc that hosts a large fault system, the Liquine-Ofqui Fault Zone, or LOFZ (Fig. 12.9). This, active since late Oligocene at least, is nearly 1200 km long and,

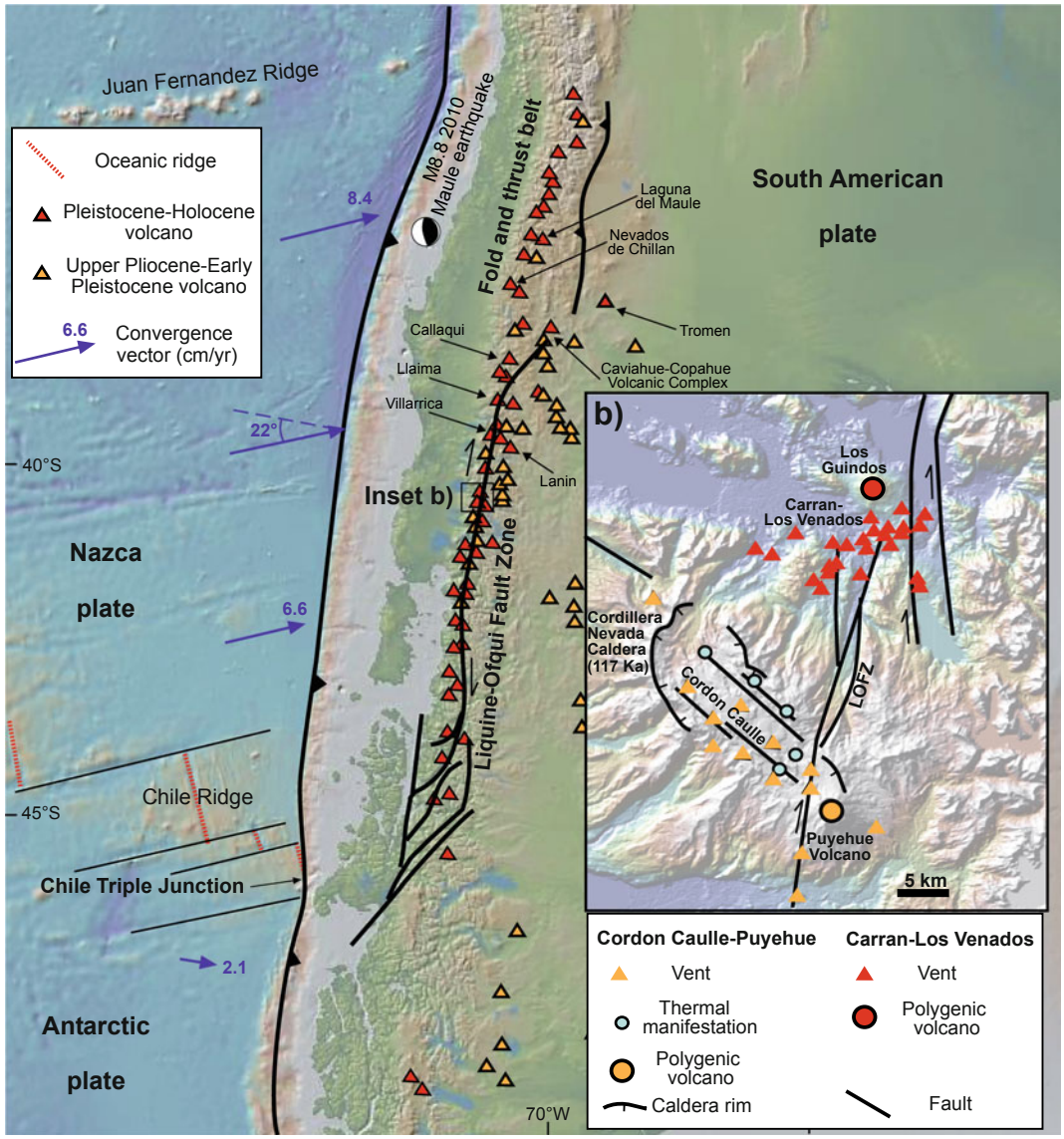

Fig. 12.9 Tectonic setting of the South Andean Volcanic Zone; location and focal mechanism of the 2010 Maule mega-earthquake are also reported. Inset b shows the structure and volcanic features of the Cordón Caulle-Puyehue and Carran-Los Venados volcanic zones (Sepulveda et al. 2005; Melnick et al. 2006; Bucchi et al. 2015). Base DEM provided by GeoMapApp

in addition to its poorly detected Quaternary dextral movement, displays a significant contractional displacement, resulting in overall transpression. The current activity of the LOFZ derives from a Quaternary NE-SW oriented maximum principal stress σ_1, with σ_2 and σ_3 mutually alternating along-strike because of local or regional factors (inherited discontinuities, variations in the convergence angle, topography) and locally producing transpressional or even contractional tectonics and seismicity (Lavenu and Cembrano 1999; Rosenau et al. 2006; Cembrano and Lara 2009; Lara et al. 2010; Legrand et al. 2011). Crustal thickness underneath the volcanic arc decreases steadily from ~50 km at 33 °S to ~35 km at 46 °S, with an accompanying decrease in the average altitude of the orogen, from 5000 m to less than 2000 m (Tassara and Yánez 2003). Seismicity occurs at depths down to 40 km in the forearc and shallower than 12 km beneath the volcanic arc. Focal mechanisms indicate overall strike-slip faulting consistent with ENE-WSW shortening. More in detail, three distinctive latitudinal domains show seismicity consistent with splay faulting along branches of the LOFZ (at its northern termination), along ENE-WSW and ESE-WNW transverse faults (in the central portion) and focused along the master branch of the LOFZ (at its southern part). This indicates a complex strain compartmentalization pattern within the arc, where variable strike-slip faulting dominates over dip-slip motions (Sielfeld et al. 2019).

Magmatic activity focuses along the LOFZ and its intersection with inherited oblique structures, developing the ~N-S trending volcanic arc. The average magma extrusion is here close to 10–13 km^3/km/Ma, although the productivity appears discontinuous (e.g., Volker et al. 2011). The South Andean Volcanic Zone includes at least 60 historically and potentially active main stratovolcanoes, as well as three large silicic caldera systems and numerous minor eruptive centres. The erupted magmas include basalts, basaltic andesites, andesites, dacites and rhyolites. The more evolved rocks have the same isotopic composition of the more primitive rocks, indicating that they formed either by crystal-liquid fractionation without assimilation, or assimilated young, isotopically similar crust, such as Miocene plutonic rocks (Stern 2004, and references therein). At the arc-scale, regional tectonics would control whether basaltic magmas reach the surface or evolve to more differentiated products. In particular, NE-SW striking volcanic alignments contain mainly basaltic to basaltic andesite compositions. Conversely, NW–SE striking alignments contain a wide range of compositions, including rhyolites (Cembrano and Lara 2009).

The central part of the LOFZ, at ~41 °S, displays interesting structural and volcanic features that may be representative of the more general tectono-magmatic relationships along the arc. This area includes the Carrán–Los Venados volcanic field and the neighbour polygenetic Puyehue–Cordón Caulle volcanic complex (Fig. 12.9; Lara et al. 2006; Singer et al. 2008; Bucchi et al. 2015). The Carrán–Los Venados volcanic field is a basaltic to basaltic andesitic volcanic field composed of 65 post-glacial scoria cones and maars and a stratovolcano. The NE-SW elongation of its feeding system, subparallel to the current maximum principal stress σ_1, suggests a zone of local extension. Petrologic data indicate that here magmas differentiate in low crustal reservoirs, followed by rapid ascent to the surface, with a post-glacial magma flux of ~3.1 km^3/ka. The Puyehue–Cordón Caulle volcanic complex consists of a NW–SE elongated 13 × 6 km wide depression hosting the NW–SE trending Cordón–Caulle area of rhyolitic fissure volcanism and the Puyehue stratovolcano to the east. The Cordón Caulle area experienced notable uplift between 2012 and 2015, partly overlapping with the 2011–2012 rhyolitic eruption (Jay et al. 2014; Delgado et al. 2016, 2019). The NW–SE elongation of the feeding system of the Puyehue–Cordón Caulle volcanic complex, perpendicular to the maximum principal stress σ_1, suggests a zone of local contraction. Here the magmas stagnate and differentiate in lower and upper crustal reservoirs, with an average magma flux similar to that of Carrán–Los Venados, although reaching more than twice its value (~9 km^3/ka) during peak

eruptive periods. Therefore, at Carrán–Los Venados monogenetic volcanism results from an extensional/transtensional regime that favours rapid magma rise without storage and differentiation in upper crustal reservoirs. Conversely, at Puyehue–Cordón Caulle, contractional deformation and transient high magma flux developed stable upper crustal silicic magma reservoirs feeding polygenic evolved volcanism (Fig. 12.10; Bucchi et al. 2015).

The tectono-magmatic features described for Carrán–Los Venados and Puyehue–Cordón Caulle may be applicable also to other volcanoes along the LOFZ (Folguera et al. 2004). For example, at the northern termination of the Liquine-Ofqui Fault Zone lies the Caviahue-Copahue Volcanic Complex, active within a 20 × 15 km wide depression in the last ~4 Ma. Here magmatic centres and hydrothermal paths have a preferred ENE-WSE alignment, parallel to the direction of the maximum principal stress σ_1. A similar structural setting is found also in the nearby ENE-WSE elongated Callaqui stratovolcano, to the west, and the NE-SW elongated Llaima stratovolcano, to the south (Melnick et al. 2006; De Maisonneuve et al. 2012; Sielfeld et al. 2017). Conversely, other nearby stratovolcanoes are aligned along a NW–SE direction, as for example Villarrica, Quetrupillan and Lanin (Fig. 12.11). All these features suggest recurrent convergence-parallel and convergence-orthogonal structural controls on the volcanoes along the South Andean Volcanic Zone, although more data are needed to generalize any behaviour.

The different tectono-magmatic conditions shown by Carrán–Los Venados and by Puyehue–Cordón Caulle may be explained by the transient variations imposed by seismic cycles associated with mega-earthquakes along the convergent plate boundary. In particular, in the inter-seismic period, the ENE-WSW trending maximum principal stress σ_1 deriving from the convergence is subparallel to the plumbing systems of the NE-SW trending volcanic alignments; this promotes local extension and rapid magma ascent through NE-SW trending feeder dikes. The maximum principal stress σ_1 is also perpendicular to the plumbing system of the NW–SE trending volcanic complexes, promoting local contraction and thus magma stagnation in sills. In the co- and post-seismic periods, that is during and immediately after mega-earthquakes, the situation may

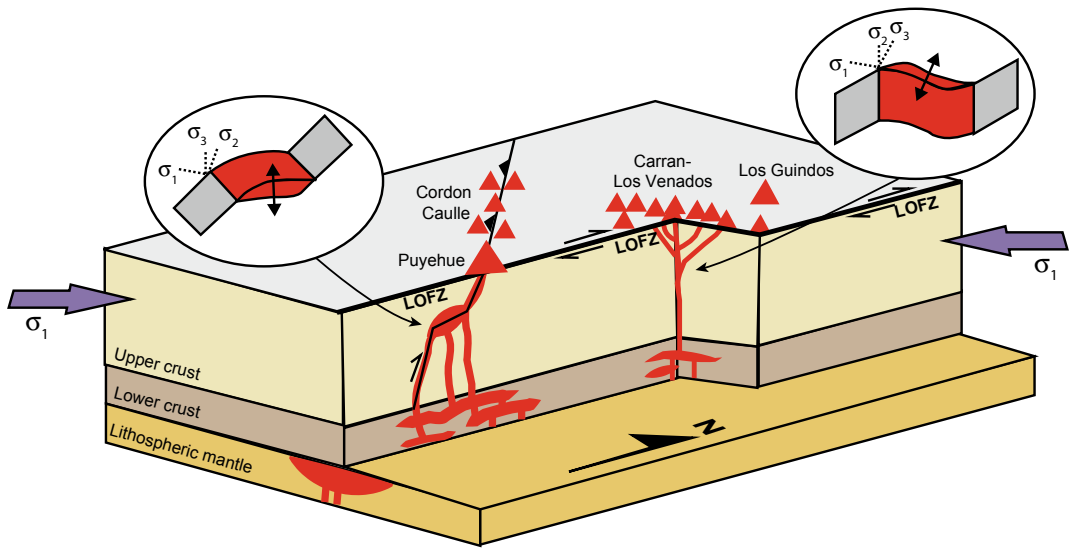

Fig. 12.10 Schematic diagram summarizing the tectono-magmatic features of the Cordón Caulle-Puyehue and Carran-Los Venados volcanic complexes in the South Andean Volcanic Zone (location in Fig. 12.9). The former lies along a NW–SE trending thrust zone, in whose flat parts magma accumulates at depth. The latter lies along a NE-SW extensional zone along the LOFZ, which promotes the rise of magma to the surface (Bucchi et al. 2015)

Fig. 12.11 View of a portion of the South Andean Volcanic Zone showing the Quetrupillan and Lanin (background) volcanoes seen from the top of Villarrica volcano. These three stratovolcanoes form a second-order NW–SE trending alignment within the N–S trending volcanic arc

be reversed, with the upper plate moving trenchward and inducing an overall arc-orthogonal (E-W to NE-SW trending) extension (Walter and Amelung 2007). As a result of this transient extension, a general increase in the eruption rate along the South Andean Volcanic Zone has been recognized in the last centuries soon after major thrust earthquakes along the plate boundary. Eruption locations imply that these effects may manifest up to several hundreds of kilometres beyond the limits of the earthquake rupture zone, with both dynamic and static stress changes affecting eruption-triggering processes over timescales of several months (Watt et al. 2009). This increase in the eruptive rate is explained by the co- and post-seismic transient extension enhancing magma ascent through NW–SE trending dikes feeding NW–SE elongated or aligned volcanoes. The latter condition may justify the Quaternary extension locally experienced by the Puyehue–Cordón Caulle Complex (Sepulveda et al. 2005). Also, the NW-SE trending 1960 rhyodacitic fissure eruption in the Cordón Caulle Complex was activated by the greatest recorded subduction zone earthquake (*M9.5*), starting 38 h after the main shock, 240 km inland (Lara et al. 2004). More recently, the 2010 *M8.8* Maule mega-earthquake induced subsidence of up to 15 cm in five volcanic areas in the South Andean Volcanic Zone within weeks of the earthquake, without detectable thermal changes. This deformation may be related to the co-seismic release of fluids from hydrothermal systems documented at three of the five subsiding volcanic areas. Among these is the Nevados de Chillan Volcanic Complex, which erupted in 2015 along a NW–SE trending fissure, perhaps reactivating a pre-existing basement structure unclamped by the Maule earthquake (Pritchard et al. 2013; Bonali et al. 2015; Lupi et al. 2020).

The northern termination of the transpressive Liquine-Ofqui Fault Zone is connected through a transfer zone to a major N-S trending back-arc thrust system. This contractional back-arc zone is characterized, at a latitude of ~37°, by several polygenic volcanoes. Among these is Tromen volcano, with the nearby intrusive complex of Cerro Negro de Tricao Malal. While the former is E-W elongated, parallel to the local direction of compression, the latter has an overall N-S elongation, parallel to the axis of the folds in the basement. In both cases, the location of the feeder dikes at the anticlinal hinges of the N-S trending basement folds suggests that dike propagation was controlled by local and shallow stresses related to the stretching of the outer portion of the folds; this mechanism may be

responsible for the vertical partitioning of igneous plumbing systems in contractional settings (Galland et al. 2007; Gurer et al. 2016).

Finally, recent studies also consider the possible effect of the climate change-driven deglaciation after the last glacial maximum along the South Andean Volcanic Zone (Mora and Tassara 2019). The resulting changes in pressure at upper crustal levels (<10 km depth) at the scale of several hundred years are of the order of 10–100 MPa. This large decompression may easily surpass the tensile strength of rocks (5–20 MPa), promoting the failure of the reservoir walls, dike propagation and the collapse of the reservoirs accompanying explosive eruptions.

12.3.2 Sumatra, Indonesia

The island of Sumatra (Western Indonesia) exposes part of the highly oblique ($\phi > 45°$) convergence resulting from the Indian plate subducting northward below the Eurasian plate along the NW–SE trending trench. The convergence velocity along the boundary increases towards southeast, from ~5 to ~6 cm/year (Fig. 12.12). This configuration results from the Cenozoic collision of India with Asia, which induced the progressive clockwise rotation of the western portion of the former Sunda subduction zone, whose non-rotational portion remains currently preserved in the island of Java (central

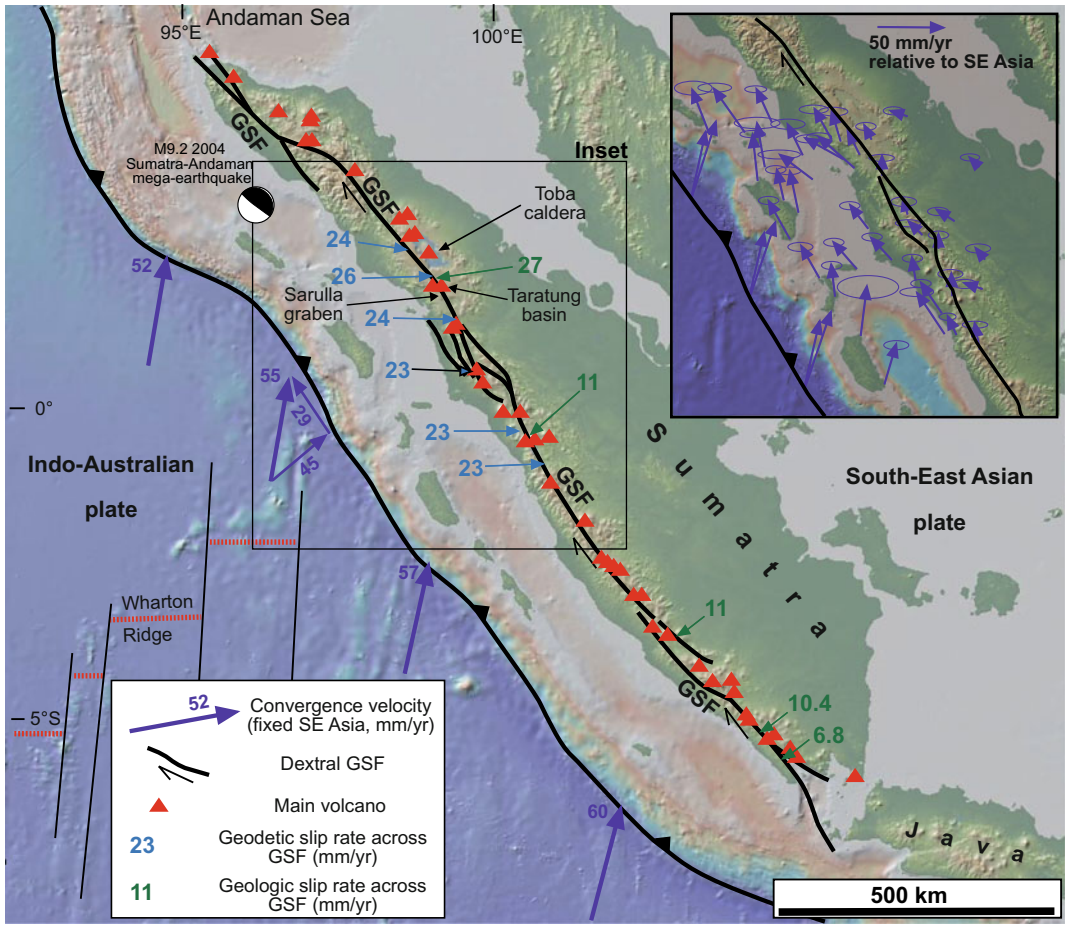

Fig. 12.12 Tectonic setting of Sumatra, Indonesia, with the geologic and geodetic slip rates along the Great Sumatra Fault (GSF) from Natawidja and Triyoso (2007); location and focal mechanism of the 2004 Sumatra–Andaman mega-earthquake are also reported. Inset shows the inter-seismic motion from GPS data between 1989 and 1996 in the central-northern part of the island (McCaffrey et al. 2000). Base DEM provided by GeoMapApp

Indonesia). The rotation increased both the obliquity of convergence and the rate of strike-slip motion along the plate boundary in western Indonesia. The Indo-Australian plate currently subducts beneath Sumatra with a complex geometry. This is highlighted by the steepening of the slab from the north (with a slab dip <60°), where it lies on the 660 km deep upper mantle discontinuity, to the south (dip >70°), where the slab pierces through the upper mantle discontinuity. Also, the slab shows a marked bend in map view in northern Sumatra, approximately below Toba caldera (Pesicek et al. 2008).

While contraction dominates in the offshore portion of the convergent plate boundary, the NW–SE trending dextral Great Sumatra Fault (GSF) focuses most of the inland deformation. The dip-slip motion towards the trench side of the overriding plate and the strike-slip motion along the arc highlight an almost full partitioning of the strain (Fig. 12.12; Bellier et al. 1999; McCaffrey et al. 2000; Bradley et al. 2017). The GSF separates the eastern basin, a region that is part of the Sunda Shelf and undergoes little internal deformation, from the western coastal areas of the forearc sliver. Analysis of well borehole breakouts, focal mechanisms of earthquakes and geologic stress indicators indicates that the regional maximum principal stress σ_1 adjacent to the GSF is oriented at a high angle to the fault (Mount and Suppe 1992). The GSF propagated southwards, in central-southern Sumatra, from $\sim$2 Ma and it is usually active as a vertical plane down to depths of $\sim$15 km, as revealed by the associated seismicity arriving nearly to the base of the brittle crust. The fault zone is segmented and consists of at least 19 major NW–SE trending subparallel branches, also forming strike-slip duplexes, with a northward increase in segment length and in slip rate, from 0.5 to 2.6 cm/year. Overall, most (>80%) of the GSF consists of a narrow (a very few km wide) zone of deformation along a main dextral segment. Limited parts (<20%) of the GSF may show offset segments, at times overlapping. Geomorphic offsets along the fault range as high as 20 km and may represent only the most recent displacement, with other unidentified structures having accommodated the dextral component of oblique convergence in the past. Interaction between dextral segments offset in an en-echelon dextral configuration creates repeated areas of localized extension along the GSF in a context of overall NNE-SSW trending maximum compression (Duquesnoy et al. 1996; Genrich et al. 2000; Prawirodirdjo et al. 2000; Sieh and Natawidjaja 2000; Natawidjaja and Triyoso 2007; Weller et al. 2012; Ito et al. 2016). As mentioned, the activity of the GSF is accompanied by seismicity, locally interrupted in volcanic areas. For example, a narrow seismic gap highlighted the volcanic areas during the aftershock sequence of the 1994 *M6.8* Liwa earthquake, in southern Sumatra, suggesting that the rupture process is also controlled by the presence of magma (Widiwijayanti et al. 1996). More in general, seismicity predominates along the plate boundary, with important effects on the overriding plate. In fact, GPS data in the northern part of Sumatra show that the co- and post-seismic displacement after the 2004 *M9.2* Sumatra–Andaman mega-earthquake, occurred offshore, was characterized by the southwest motion of the volcanic arc region, consisting of several tens of centimetres of co-seismic displacement, plus tens of centimetres in the first year after the earthquake. The 2004 mega-earthquake was followed, one month later, by a seismic swarm and a submarine eruption in the Andaman Sea, along the northern continuation of the Sumatra arc. This seismicity is consistent with the regional tectonic setting and the involvement of fluids, also magmatic, producing arc-parallel normal faults (Subarya et al. 2006; Gahalaut et al. 2008; Shearer and Burgmann 2010; Kamesh Raju et al. 2012; Kundu et al. 2012).

Arc volcanism has been accompanying convergence at least from the Mesozoic. While the late Miocene volcanism in northern Sumatra is scattered, in the southern part it generally overlaps with the Quaternary volcanism, although the latter may be slightly more shifted to the west. Part of the Quaternary volcanism focuses along the GSF (Fig. 12.12). Quaternary volcanics are mainly calcalkaline andesites, dacites and rhyolites, with genetically homogeneous overall composition; relatively primitive rocks, as basalts, are rare, with even the most primitive lavas suffering crustal contamination (Gasparon 2005). The volcanic arc consists of approximately 50 major volcanoes. Most of these are stratovolcanoes or composite volcanic edifices between 600 and 3800 m high, with monogenic vents on their flanks. At times, calderas are present: Toba caldera is the largest and most representative volcanic complex, located above a tear in the bent subducting plate. Toba is the site of Earth's largest Quaternary eruption, ejecting $\sim$3000 km^3 of magma at $\sim$75 ka (Fig. 5.5; Chesner 2012; de Silva et al. 2015; Koulakov et al. 2016). The caldera has a pronounced NW–SE elongation, parallel to the nearby GSF segment, and this configuration has been interpreted as due to a presently inactive stepover between dextral segments. However, the structural relationships between the GSF segment and the caldera structure are not obvious. In fact, the GSF segment lies $\sim$10 km to the southwest of the western caldera rim, and geodetic modelling shows that slip of the GSF segment currently focuses several kilometres southwest of the geologic fault plane. The magma reservoir below the caldera consists of stacked sills down to a depth of 7 km, lying on top of a low velocity anomaly almost extending down to the slab (Detourbet et al. 1993; Genrich et al. 2000; Stankiewicz et al. 2010; Chesner 2012; Jaxybulatov et al 2014). Other volcanic areas, in addition to stratovolcanoes and calderas, host domes and geothermal activity. In the geothermal areas of the Sarulla graben and the Tarutung Basin the fluid pathways are related to pull-apart structures, negative flowers and subvertical splays of the GSF. In the latter case, the geothermal reservoirs are centred along the fault zone, where the highly fractured and hydrothermally altered rocks serve as main conduits for vertical fluid flow from deeper magmatic sources (e.g., Moore et al. 2001).

Despite the apparent spatial coincidence between most volcanoes and the Great Sumatra Fault (Fig. 12.12), closer inspection suggests that the location and the eruption rate of many volcanoes are not really controlled by the activity of the dextral GSF (Fig. 12.13). Rather, the volcanoes mainly lie above a consistent depth of the slab below, at 130 $\pm$ 20 km. Indeed, the slab-derived fluid-rich portion of the asthenospheric wedge seems to control the location of both the volcanic arc, through partial melting, and of the GSF, through magma-induced thermal weakening able to localize faulting in the upper crust. The latter feature is supported by the different timing in the development of the GSF along Sumatra. In fact, the more recent central-southern portion of the GSF formed in the last 2 Ma, postdating the older Miocene volcanism. The fact that the latter is found in the same location as the Quaternary volcanism indicates that the Miocene arc was not controlled by the activity of the GSF and suggests that a similar condition applies also to the Quaternary arc. Overall, this implies that the magmatic arc controls the location of plate deformation, although once a major fault zone is established its activity may further promote the rise and shallow emplacement of magma (McCaffrey et al. 2000; Sieh and Natawidjaja 2000; Acocella et al. 2018).

Even though not particularly related to the activity of the GSF, the current volcanic arc also experiences a convergence-orthogonal direction of extension, which is kinematically compatible with the dextral systems of the GSF and explains the common $\sim$NNE-SSW elongation and/or alignment of many volcanoes (Fig. 12.14). However, there is also evidence of subordinate arc-normal extension, as suggested by structural data and volcano elongations, which may be related to a transient co- and post-seismic stress field inversion induced by mega-earthquakes, as observed for the 2004 event. Also, volcanic activity is largely confined within the volcanic

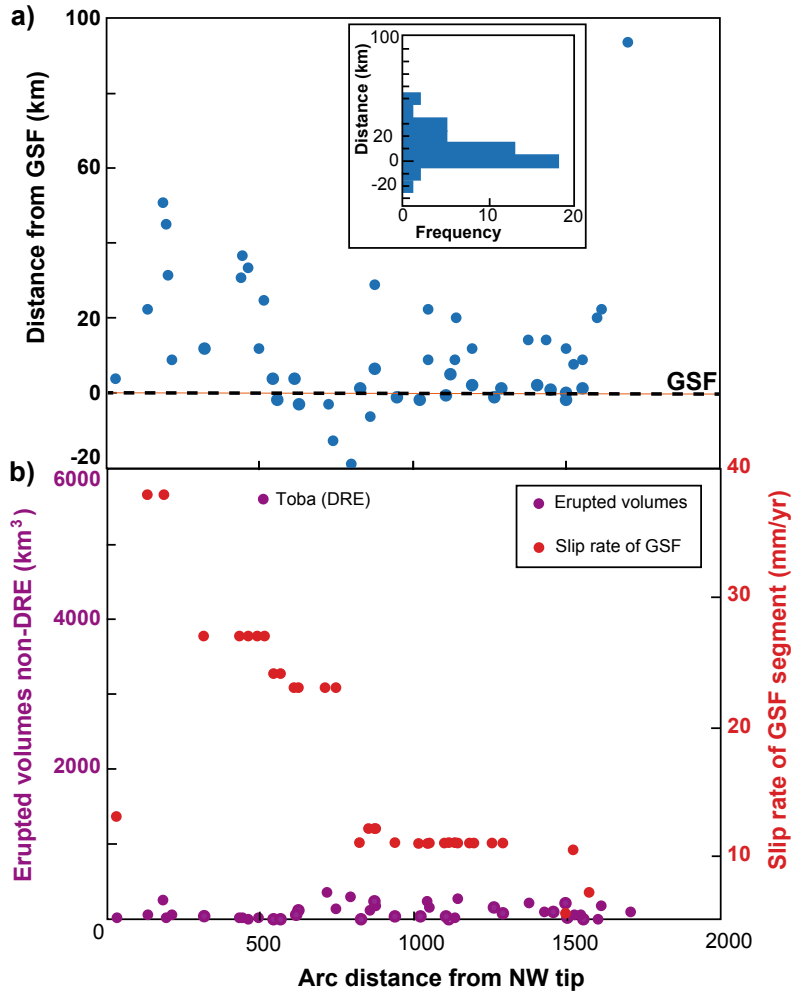

Fig. 12.13 **a** Distribution of volcanoes along Sumatra (from northeast, to the left, to southwest, to the right) as a function of the distance from the Great Sumatra Fault (GSF); **b** Non-DRE (Dense Rock Equivalent, except for Toba) erupted volumes and GSF slip rates along the Sumatra arc, from northeast, to the left, to southwest, to the right (modified after Acocella et al. 2018)

edifices, with limited evidence of monogenic volcanism between the main polygenic volcanoes. This suggests the lack of elongated magmatic systems, implying a central, and not linear (as for example in the Taupo Volcanic Zone), mode of rise of the magma in the crust.

Overall, there is a limited control of the strike-slip structures on volcanism at Sumatra. This supports only in part previous evidence from the deeper structure of extinct and eroded magmatic arcs, where pluton emplacement has been widely associated with local extension created by strike-slip systems (see Sect. 4.5.2). This partial agreement may result from several possibilities: among these, a variable role of the arc structure at depth and at the surface, with a stronger control on magma emplacement at depth and a weaker control on the rise of the magma towards the surface. A similar behaviour has been postulated for the central Aeolian Volcanic Arc of southern Italy. However, conversely to Sumatra, along the central Aeolian Arc there is evidence of magmatism continuing, through eruptive fissures, outside the main volcanoes, suggesting the activity of magmatic systems; these may be induced by a variation in the shallower tectonic regime, which becomes extensional (Ruch et al. 2016; Acocella et al. 2018).

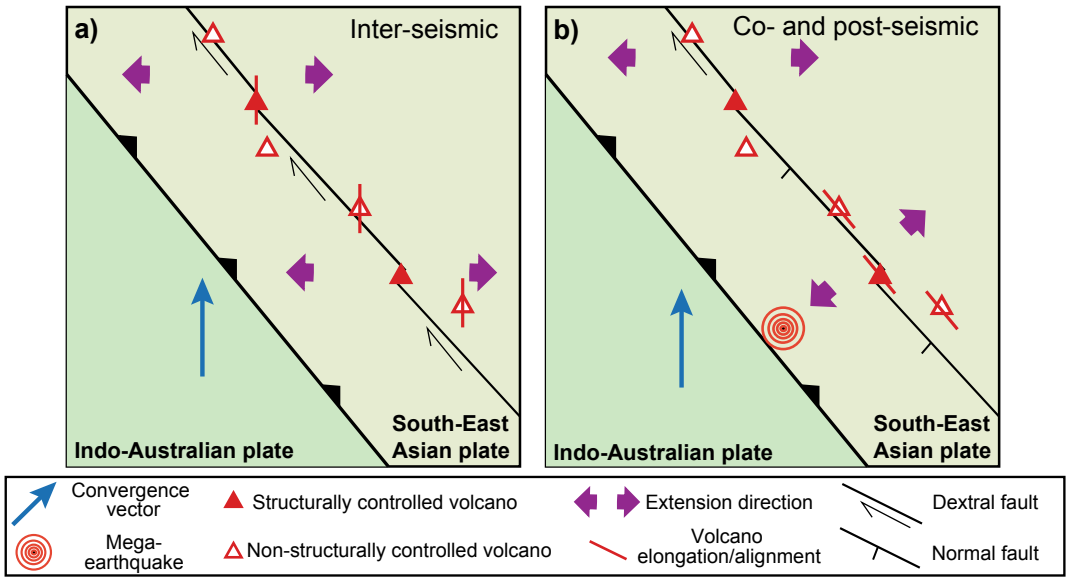

Fig. 12.14 Tectono-magmatic relationships along the Sumatra obliquely convergent volcanic arc. **a** During the inter-seismic period the arc is characterized by the activity of dextral structures associated with strain partitioning. Part of these structures may control the location of the volcanoes ("structurally controlled volcano"). The location of other volcanoes ("non-structurally controlled volcano") away from the strike-slip zone may be explained by other factors, as slab depth or convergence-orthogonal extension, controlling also volcano alignment and elongation. **b** During transient conditions (as in co- and post-seismic periods due to the activity of mega-earthquakes) the arc may undergo arc-normal extension, with the local reactivation of the strike-slip faults as normal faults; the alignment and elongation of volcanoes may partly reflect these transient conditions, becoming subparallel to the arc (modified after Acocella et al. 2018)

12.4 Contractional Arcs

Contractional volcanic arcs are characterized by dominant shortening, resulting from overall arc-orthogonal compression, a condition imparted by orthogonal convergence. As most plate boundaries do not experience pure orthogonal convergence, a frequent and non-negligible strike-slip component is often associated with contractional arcs. Indeed, only very few volcanic arcs experience evident and dominant contraction, and negligible strike-slip motion: among these are the eastern Aleutian Arc, the northeast Japan Arc and, for much of its late Cenozoic-Quaternary evolution, the more complex arc of the Central Andes (Table 12.1; Acocella and Funiciello 2010). Below the focus is on the most-studied and representative volcanic arcs of northeast Honshu (Japan; Sect. 12.4.1) and the Central Andes (Sect. 12.4.2).

12.4.1 Northeast Honshu, Japan

Honshu is the largest island in Japan. The northeast Honshu volcanic arc lies to the west of the N-S trending Japan trench, where the westward Pacific plate subducts with a N115° motion of ~8 cm/year. To the north, the Japan trench is connected to the NE-SW trending Kuril trench. Here the oblique convergence of the Pacific plate induces the arc-parallel southwest motion of the Kuril forearc sliver, colliding in east Hokkaido. To the south, the Japan trench is connected to the N-S trending Izu-Bonin trench, where the Pacific

plate subducts below the Philippine Sea plate. To the west lies the Japan Sea, a Miocene back-arc basin associated with widespread basaltic volcanism (Fig. 12.15; Kimura 1986; De Mets 1992; Kimura 1996; Yoshida et al. 2013).

The ~400 km long, N-S trending volcanic arc of northeast Honshu focuses along the uplifted central mountainous range (Ou Backbone Range; Hasegawa et al. 1991). Here during Middle Miocene to Pliocene the regional stress field related to the convergence of the Pacific plate was neutral and not responsible for any distinct structural pattern. However, the southwest indentation of the Kuril sliver, resulting from the oblique convergence with dextral component along the Kuril Arc, imposed a southwest oriented maximum compression and major arc-parallel dextral faults in northeast Honshu. The Kuril sliver indentation may have begun at 10–12 Ma, as a consequence of a change in motion of the Pacific plate. The Middle Miocene to Pliocene northeast Honshu Arc produced bimodal volcanism, with rhyolites and subordinate low K basalts focusing along the Ou

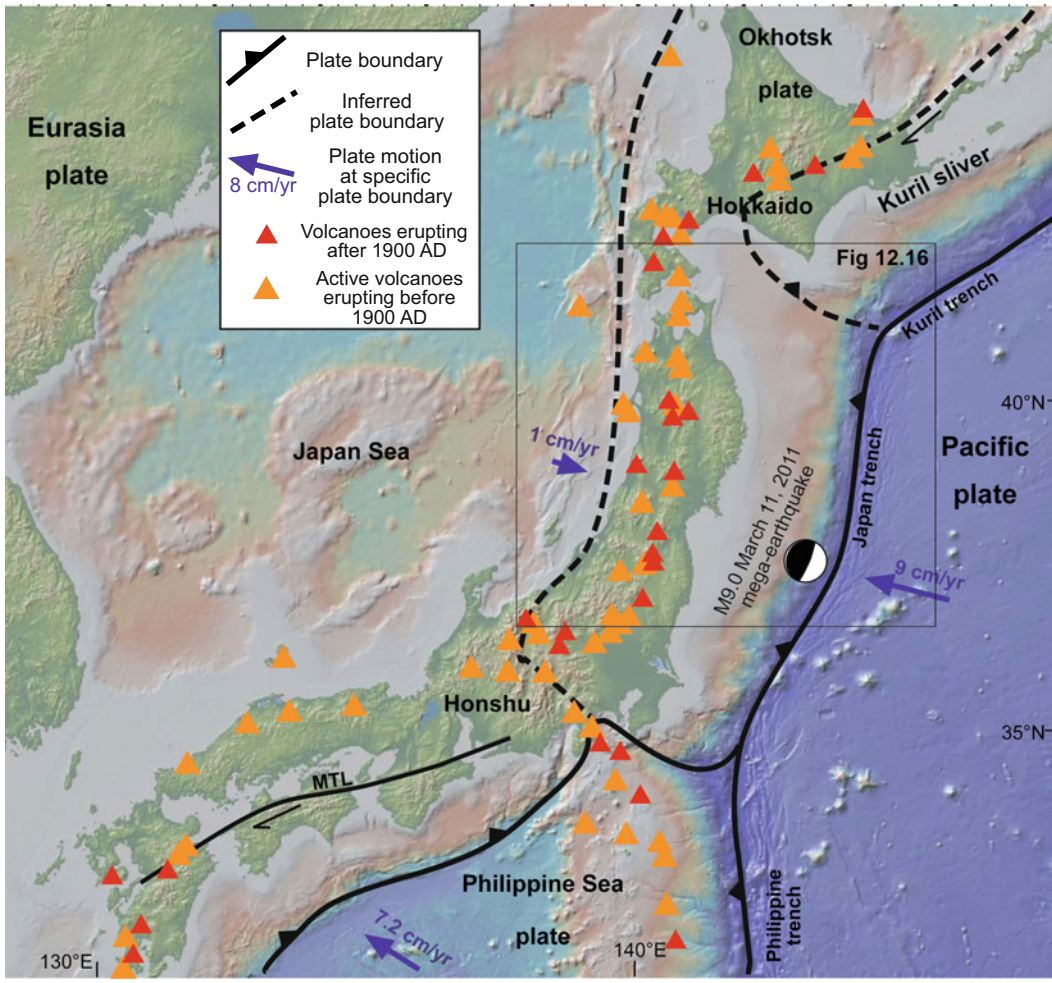

Fig. 12.15 Tectonic setting of northeast Honshu (Japan), with the major active volcanoes. Solid lines: subduction front; dashed lines: inferred boundaries of minor plates. MTL = Median Tectonic Line in southwest Japan. Plate motions from Gripp and Gordon (2002). Location and focal mechanism of the March 11, 2011 Tohoku mega-earthquake are also reported. Base DEM provided by GeoMapApp

Backbone Range, where nearly eighty calderas were fed by felsic plutons following crustal heating and re-melting. The volcanic productivity was approximately 210 km^3 per Ma per 200 km of length of the arc (Fig. 12.16; Sato 1994; Kimura 1996; Yoshida 2001; Acocella et al. 2008; Yoshida et al. 2013). In this period, magma rose and erupted mainly along NE-SW trending areas parallel to the direction of compression imposed by the Kuril sliver. These areas where probably associated in location and orientation with localized extension created by the active arc-parallel dextral faults. These extensional areas also had a different orientation, and were thus uncoupled, from the ~E-W trending paths which have been focusing the rise of melts from the slab in the mantle below the arc in the last 13 Ma (Tamura et al. 2002).

A change in the stress field around the Pliocene–Quaternary boundary resulted in an ~E-W oriented direction of maximum compression, possibly related to the increase in the motion of the Pacific plate (Pollitz 1986). This developed two N-S trending uplifted zones, bounded by reverse faults, in northeast Honshu: the Ou Backbone Range (to the east) and the Dewa Hills (to the west). N-S trending reverse faults become active, also bordering the thermally anomalous part of the crust coinciding with the magmatic arc. The present ~E-W oriented arc-perpendicular compression at crustal levels is supported by various geophysical and geodetic data. This compression is evident also below the arc, were the direction of mantle shear-wave polarization anisotropy is ~E-W oriented, consistent with finger-like mantle diapirs. During Quaternary, the composition of volcanism largely consisted of calcalkaline andesite, erupted from approximately 60 stratovolcanoes, with more evolved compositions being restricted to approximately ten calderas. These stratovolcanoes are also ~E-W aligned and elongated, forming a distinct subpattern with regard to the ~N-S trending one observed at the arc-scale (Fig. 12.16; Ito et al. 2000; Igarashi et al. 2001; Tamura et al. 2002; Nakajima and Hasegawa 2004; Kato et al. 2006; Loveless and Meade 2010). A few of these volcanoes, as Zao, show in the last 2 ka much lower intrusive to extrusive ratios than those estimated for other volcanoes of northeast Honshu, probably following a different thermal and rheological state of the crust (Zellmer et al. 2019).

The Quaternary deformation pattern associated with the volcanoes mostly consists of arc-parallel thrust faults and subordinate arc-perpendicular normal faults, extension fractures and eruptive fissures. These arc-perpendicular extensional structures may result from: a) the shallow propagation and emplacement of E-W trending dikes, parallel to the regional maximum principal stress σ_1; (b) the accumulation of stacked sills, locally increasing the vertical component of the principal stress, which passes from σ_3 to σ_2 and σ_1, and with the arc-parallel oriented σ_2 becoming σ_3 (Fig. 10.24b). Condition b promotes the accumulation of large volumes of magma and is consistent with crustal thickening and the widespread magma-driven uplift along the magmatic arc (Acocella et al. 2008; Yoshida et al. 2013; George et al. 2016). The Quaternary E-W trending structures and the E-W elongation and alignment of volcanoes may be thus considered as the shallowest expression of the ~E–W trending hot mantle fingers imaged at depth, suggesting a Quaternary coupling in the rise of magma from the upper mantle to the upper crust. This possibility is supported by the spatial coincidence between the distribution of the volcanic areas along the Ou Backbone Range and the Dewa Hills and the local negative Bouguer gravity anomalies along the Japan Sea side of the volcanic arc and the low velocity regions in the mantle wedge. The connection between these areas at different depth is confirmed by distinct low velocity regions indicative of partial melting that are continuously distributed from the mantle wedge to the middle crust just below the Ou Backbone Range (Fig. 12.16; Tamura et al. 2002; Acocella et al. 2008; Okada et al. 2010; Yoshida et al. 2013). This coupling leads to a two-dimensional mantle wedge flow, ensuring higher temperatures in the shallow part of the wedge and higher productivity of mafic magma.

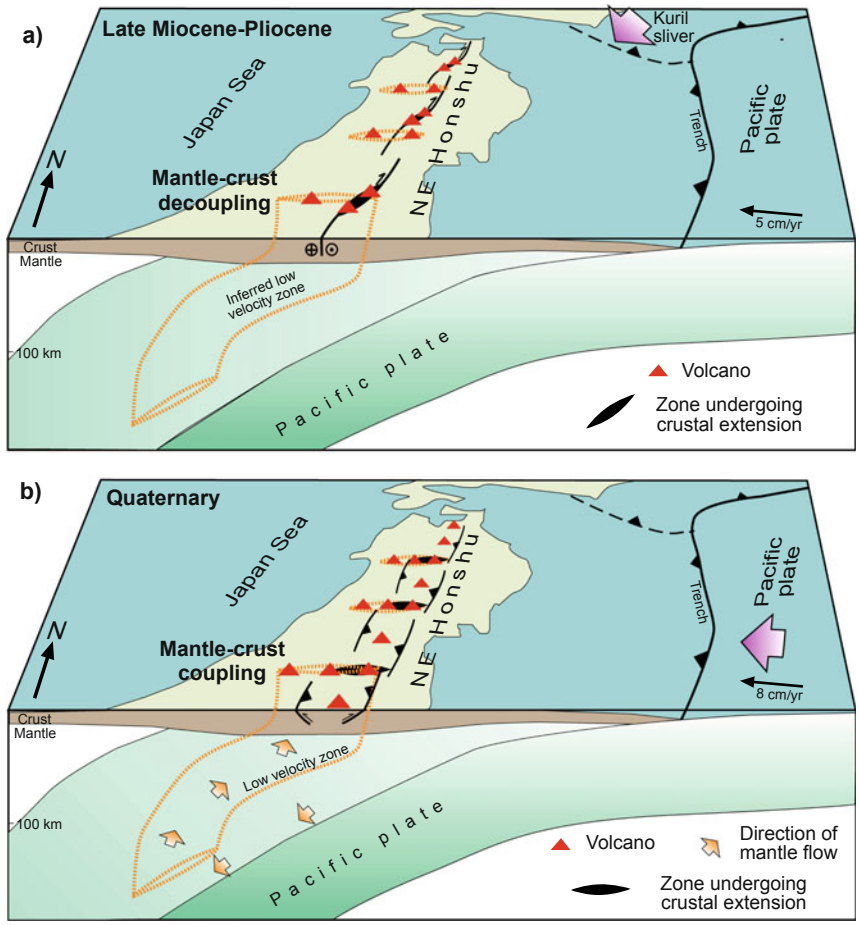

Fig. 12.16 Summary of the tectono-magmatic features of late Miocene-Pliocene (**a**) and Quaternary (**b**) in northeast Japan (modified after Acocella et al. 2008). **a** During late Miocene-Pliocene, the N-S- and NE-SW trending paths for the rise of magma in the crust induced by the indentation of the Kuril sliver (black wedges) are uncoupled with the ~E–W trend of the melts rising in the mantle (dashed orange ellipses); this generates a bimodal volcanism, with lower erupted volumes per Ma. **b** During Quaternary the ~E–W trending paths for the rise of magma in the crust under orthogonal convergence are coupled with those of ~E–W trending hot mantle fingers. The connection between deeper mafic and shallower felsic magmas generates higher volumes of calcalkaline andesites

At crustal levels, the mixing between the deeper mafic and the shallower felsic magma generates the andesites. The Quaternary andesites are associated with larger erupted volumes (approximately 310 km^3 per Ma per 200 km of length of the arc) than the volumes of rhyolites erupted during Miocene-Pliocene. This feature, ultimately attributed to major changes in plate interactions, indicates that pure convergence does not hinder volcanic activity. Rather, under conditions of mantle-crust coupling, magmatic and volcanic activity may be even enhanced (Acocella et al. 2008; Yoshida et al. 2013; Wada et al. 2015; Mahony et al. 2016).

The 2011 *M9.0* Tohoku mega-earthquake caused impressive crustal deformation in northeast Honshu, with significant co-seismic, as well as post-seismic, arc-perpendicular extension across the volcanic arc, reversing the inter-seismic arc-perpendicular contraction (Fig. 12.17). This motion is the transient expression of the trenchward movement of the

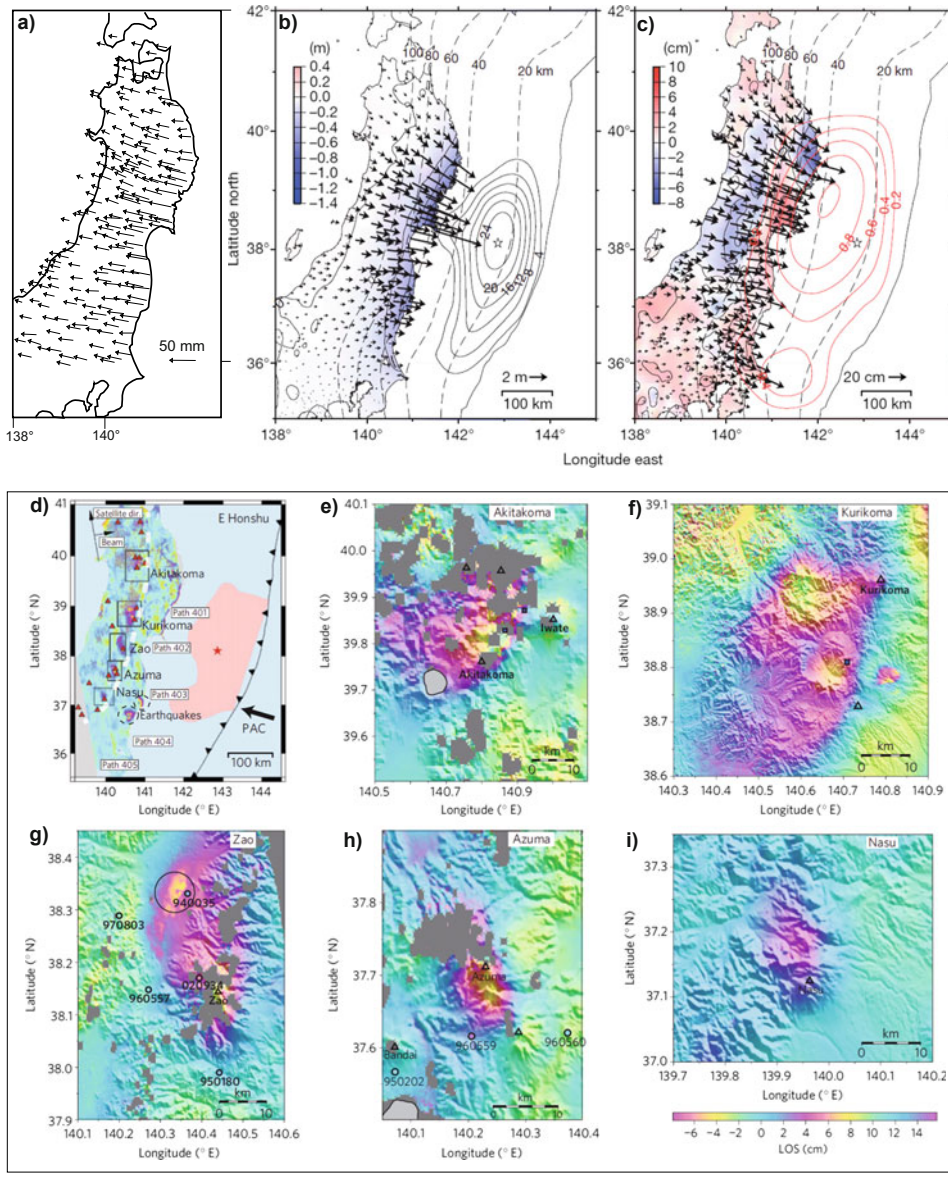

Fig. 12.17 Inter-seismic (**a**, 1997–2001 period), co-seismic (**b**, 10–11 March 2011) and post-seismic (**c**, 12–25 March 2011) GPS motions along the northeast Honshu Arc relative to the March 11, 2011 *M9.0* Tohoku mega-earthquake (Miura et al. 2004; Ozawa et al. 2011). **d** Overview of the subsidence occurred in several volcanic areas (**e**–**l**) in northeast Honshu in the February-April 2011 period, detected from InSAR data (Takada and Fukushima 2013)

overriding plate during and after the mega-earthquake and has been also confirmed by structural field data, which highlight the coexistence of arc-parallel normal faults and thrust faults along the arc during Quaternary, with the normal faults likely resulting from older seismic events. Despite the sharp co-seismic kinematic reversal in northeast Honshu, a minor inter-seismic component of accelerated trenchward motion was also detected in the decades before the 2011 Tohoku earthquake and related to the increased slip rate on the Japan trench plate

interface (Miura et al. 2004; Acocella et al. 2008; Ozawa et al. 2011; Mavrommatis et al. 2014). In the portion of the arc perturbed by the mega-earthquake several volcanoes subsided by 5–15 cm, forming elliptical depressions up to 15–20 km wide and N-S elongated, perpendicularly to the maximum co-seismic extension. The magmatic bodies beneath may have deformed and subsided in response to crustal stress changes or, alternatively, the enhanced crustal permeability may have promoted the escape of fluids from the overlying hydrothermal systems, similarly to what inferred after the 2010 Maule mega-earthquake in southern Chile (Takada and Fukushima 2013; Pritchard et al. 2013).

12.4.2 The Central Andes

The Central Andes provide a case of widespread and exceptional magmatism in an arc experiencing a complex evolution under dominant contraction. The Andes result from the subduction, since late Proterozoic, of the Nazca plate below the South American plate. Magmatism has been accompanying the evolution of the Andes with variable productivity, testified by the evidence that increased regional contraction (as in the Mesozoic) was associated with increase in volcanism, whereas oblique convergence with strike-slip motion (as in the Miocene) enhanced plutonism. Andean volcanism currently focuses above moderately to steeply dipping slabs (dip >25°), delimited by flat slabs portions underlying the non-volcanic parts of the orogen (Jordan et al. 1983; Grocott et al. 1994; McNulty et al. 1998).

The Central Andes magmatism includes the diffuse and voluminous late Cenozoic to Quaternary volcanism that reaches a width of ~300 km in the most thickened portion of the orogen. This volcanism is often defined as **flare-up**, referring to a phase in continental arc evolution characterized by episodic higher flux magmatism producing a large province of calderas and ignimbrites dominated by dacite to rhyolite compositions. Ignimbrite flare-up, observed also in various parts of the western United States and Mexico, requires an elevated heat supply from the mantle to generate a transcrustal magma system fuelling some of the largest silicic eruptions on Earth (Best et al. 2016; de Silva and Kay 2018, and references therein). In the Central Andes, the switch from steady state volcanism (dominantly andesite–dacite composite cones) to flare-up volcanism (dominantly large-scale ignimbrites and caldera complexes) is related to the southward migration and subduction of the oceanic Juan Fernandez Ridge, on the Nazca plate, in the last 25 Ma. The subducting warm and buoyant ridge determined the flattening of the slab below the Central Andes and the temporary lack of volcanism at the surface (Fig. 12.18). This condition coincided with an early Miocene acceleration in the rate of westward drift of South America over the Nazca plate. Both the flat subduction and the accelerated plate motion contributed to the contractional tectonic environment that produced over 300 km of Central Andean shortening, with a 50–70 km thick crust. While the southward migration of the ridge determining the flat slab correlates with a space–time gap in volcanic activity, soon after the passage of the ridge the slab increased its dip, from flat to shallow dipping, finally sweeping volcanism eastward and defining a broad volcanic footprint in the Central Andes (Oncken et al. 2006; Best et al. 2016; de Silva and Kay 2018). The steepening slab then started to roll-back, promoting decompression melting in the overlying enlarging mantle wedge, lowering its viscosity. This condition focused an elevated thermal input, encouraging crustal melting and generating a significant amount of magma. This resulted in the appearance and westward migration of volcanism from ~24 Ma, concurrent with an ignimbrite flare-up, in the Central Andes. In the southern portion of the Central Andes, the flare-up created the Altiplano-Puna Volcanic Complex, active in the last ~10 Ma and characterized by a mantle magma production rate of nearly 20 km^3/km/Ma. This complex, hosted within the Andean plateau at altitudes above 3000 m, is bordered to the west by the Andean

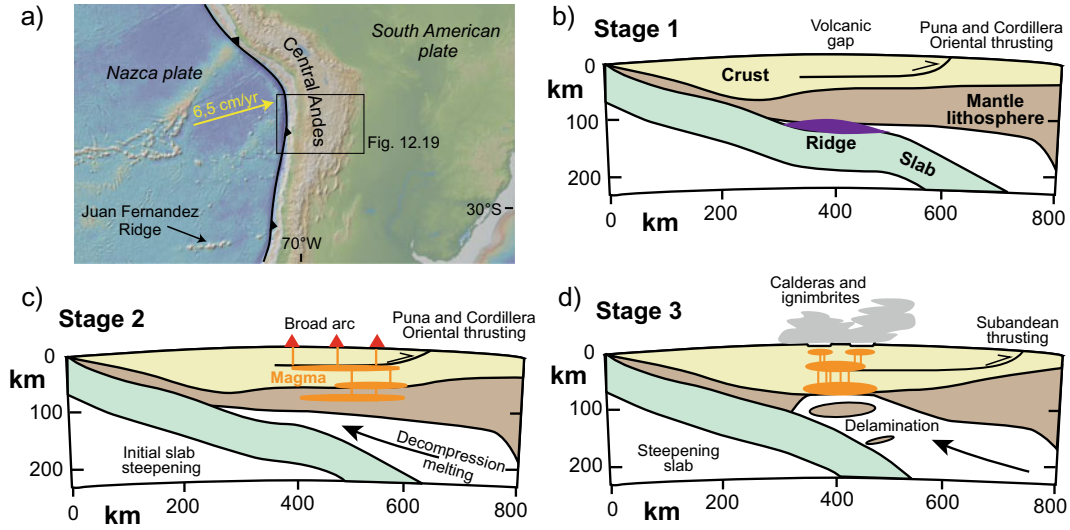

Fig. 12.18 **a** Simplified tectonic setting of the Central Andes, showing also the current location of the southward migrating Juan Fernandez Ridge; base DEM provided by GeoMapApp. **b–d** Main stages of evolution of the Central Andes in the last 25 Ma along an ideal E-W oriented lithospheric section. **b** The subduction of the Juan Fernandez Ridge induces a flat slab underlying a volcanic gap. **c** After the subduction of the ridge the steepening of the slab induces decompression melting in the overlying mantle wedge, promoting volcanism over a broad area. **d** Piecemeal delamination of the lithosphere of the southern part of the Central Andes produces a warmer asthenosphere above the slab, promoting sustained magmatic activity and ignimbrite flare-up of the Altiplano-Puna Volcanic Complex (modified after de Silva and Kay 2018)

forearc and to the east by the Eastern Cordillera and the Subandean foreland (Fig. 12.19). Episodic piecemeal delamination from late Miocene to Quaternary produced peaks in volcanic output of the Altiplano–Puna Volcanic Complex. Delamination may have affected the lower continental crust and the mantle lithosphere, both sinking into and replaced by the underlying hotter and less viscous mantle (Kay and Kay 1993; Kay and Coira 2009; Gioncada et al. 2010). Tomography has repeatedly highlighted high velocity structures beneath the Puna, interpreted as detached continental lithosphere, previously thickened and weakened by orogenic processes. The delamination may have also contributed to the uplift of the Central Andes (Schurr et al. 2006; Bianchi et al. 2013; Liang et al. 2014). Therefore, the exceptional and widespread late Cenozoic volcanic activity in the Central Andes, including the development of the Altiplano–Puna Volcanic Complex, results from decompression melting induced by slab steepening following ridge subduction and a hotter mantle wedge fuelled by warmer asthenosphere following piecemeal delamination. This complex sequence of events is responsible for the ~70 km thick crust supporting a plateau above 3000 m and the exceptional magmatism feeding the Altiplano–Puna Volcanic Complex (Fig. 12.20). Both features are described in more detail below.

The shortening, thickening and uplift of the crust in the Altiplano region began at approximately 25 Ma, following the shallowing of the slab and the increased convergence rate. The latter promoted shortening in the Eastern Cordillera and, subsequently, thrusting in the Subandean foreland to the east. Shortening and uplift in the Puna commenced 5–10 million years later and continued until Quaternary. Known shortening at the surface accounts for only 70–80% of the observed crustal thickening, suggesting that magmatic addition and other processes, such as lower crustal flow or tectonic underplating may contribute significantly to the thickening of the Central Andes (Allmendinger

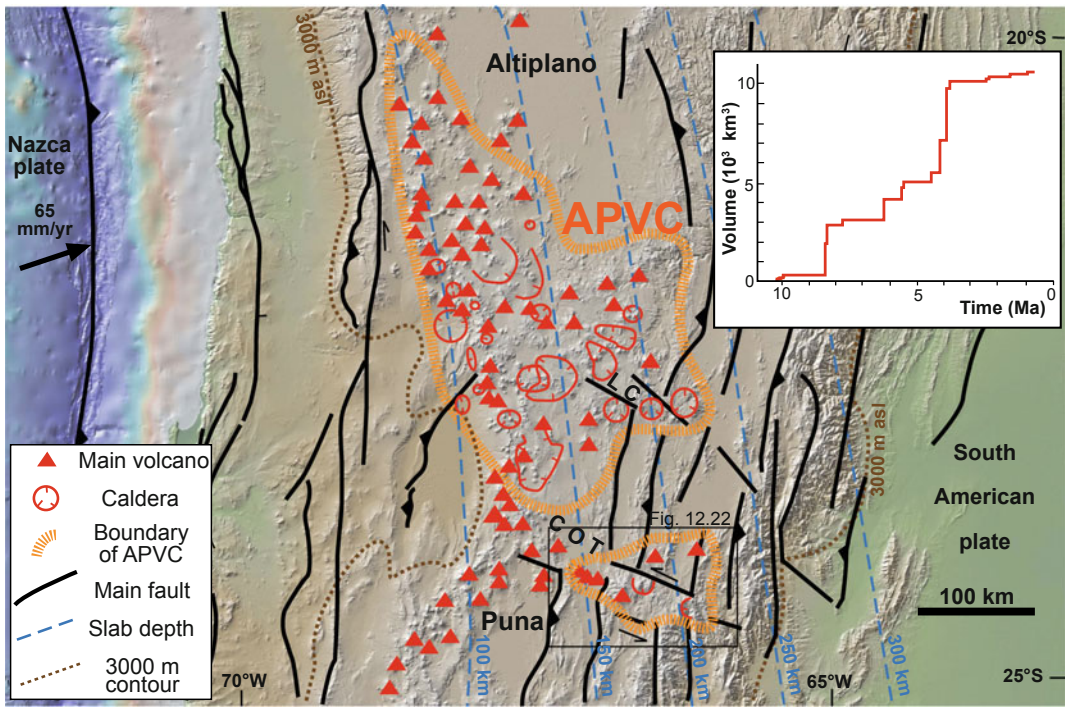

Fig. 12.19 Tectonic setting of the Altiplano–Puna Volcanic Complex (APVC), showing the current slab contours, the major fault systems, including the transverse Lipez-Coranzuli (LC) and Calama-Olacapato-El Toro (COT) fault zones, the major calderas and stratovolcanoes and the 3000 m contour of the Andean plateau (after de Silva and Gosnold 2007). Base DEM provided by GeoMapApp. Inset shows the cumulative volume versus time of major ignimbrite eruptions of the Altiplano-Puna Volcanic Complex (modified after de Silva and Gosnold 2007)

et al. 1997; Hindle et al. 2005). Since 10 Ma, the southern Puna portion of the plateau underwent pure shear deformation, whereas the northern Altiplano portion underwent simple shear. These modes of crustal thickening correlate with changes in lithospheric thickness, modes of isostatic compensation, broad wavelength topography, magmatism and slab steepening (Kay and Kay 1993; Allmendinger and Gubbels 1996; Gioncada et al. 2010).

The Puna and Eastern Cordillera regions experienced NW–SE and NE-SW trending shortening directions during Miocene-Pliocene and during the Pliocene to Quaternary, respectively. The change in the shortening direction has been related to the change in the direction and rate of motion of the South American plate, or to the variation in the orientation and kinematics of prominent fault zones. Neogene deformation also shows orogen-parallel extension propagating southward and eastward, likely induced by mid to lower crustal orogen-parallel channel flow (Marrett and Strecker 2000; Riller et al. 2001). On the Puna, the ~N-S trending high angle reverse faults responsible for a Cenozoic shortening of 10–15% have been reactivated, from late Miocene to Quaternary, with predominant dextral and minor normal motion. Also, much of the Puna has been dominated for the last 1–2 Ma by strike-slip and extensional faulting, in contrast to the protracted earlier history of thrust faulting (Cladouhos et al 1994; Tibaldi et al. 2009). However, there is evidence of ongoing Quaternary contraction along the western and eastern borders of the Puna: while to the west magma intrudes along active reverse faults, the foreland

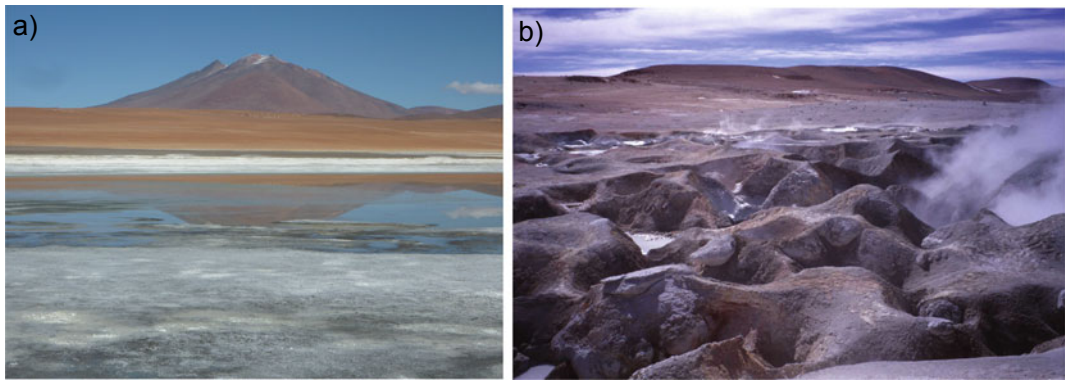

Fig. 12.20 Examples of current volcanic activity in the Altiplano-Puna Volcanic Complex of the Central Andes. **a** View of Aracar stratovolcano, in the southern Puna of Argentina, from the east. The active volcano, 6095 m high, may have last erupted in 1993. **b** View of the Sol de la Manana geothermal area in southern Bolivia, characterized by bubbling mud pots and geysers

to the east is experiencing ~E-W trending compression (Coutand et al 2001; Gonzalez et al. 2009).

Within this tectonic context, a distinct flare-up within the Neogene Central Andean ignimbrite province produced the most voluminous ignimbrite plateau in the southern half of the province from 22 to 24 °S, that is the Altiplano-Puna Volcanic Complex. Approximately 15,000 km^3 of magma were erupted in the last ~10 Ma, focusing in pulses every ~2 Ma, at 8, 6 and 4 Ma, with eruption rates one order of magnitude higher than the average rate for the flare-up of continental silicic provinces The composition of the ignimbrites includes dacites and rhyolites with minor trachydacites, andesites and latites (Fig. 12.19; Best et al 2016, and references therein). Elevated input from the mantle induced crustal melting and assimilation, developing crustal-scale intrusive complexes thermally softening the lower crust (de Silva and Gosnold 2007). A low velocity zone at a depth between 15 and 30 km has been interpreted as a sill-like magma body due to partial melting (~20%) and responsible for magmatic intraplating. This area lies above a 100 to 200 km deep zone of P-wave attenuation, connecting the volcanic areas of the plateau to the seismic zone within the slab: the connecting zone is interpreted as ascent pathway for metamorphic fluids and partial melts (ANCORP Working Group 2003; Schurr et al. 2003; Schilling et al. 2006). More recent seismic images identify a ~200 km wide and ~11 km thick low velocity zone at 4–25 km depth below sea level, interpreted as the plutonic complex that sourced the voluminous volcanics. These images show that the ~500,000 km^3 volume of this plutonic complex, or crustal-scale batholith, is one order of magnitude larger than previous estimates, retaining a significant percentage (up to 25%) of partial melt, most likely in a mush state. These images also allow making one of the best-constrained calculations of a plutonic to volcanic ratio, which is between 20 and 35 (Ward et al. 2014). Geodetic data from the last decades reveal a regional uplift of the entire Altiplano-Puna Volcanic Complex at an average of ~1.0 cm/year, whose fluctuations suggest a non-steady supply of melt and/or volatiles from the partially molten magma body below. Superimposed are more local uplifts over specific volcanic complexes, as Uturuncu and Lazufre, revealing prolonged unrest (Lau et al. 2018; Pritchard et al. 2018; Reath et al. 2019).

Magma emission in the Altiplano-Puna Volcanic Complex focused in ~20 large and complex calderas, along five NW–SE trending transverse magmatic belts, largely recognized from the alignment of magmatic centres,

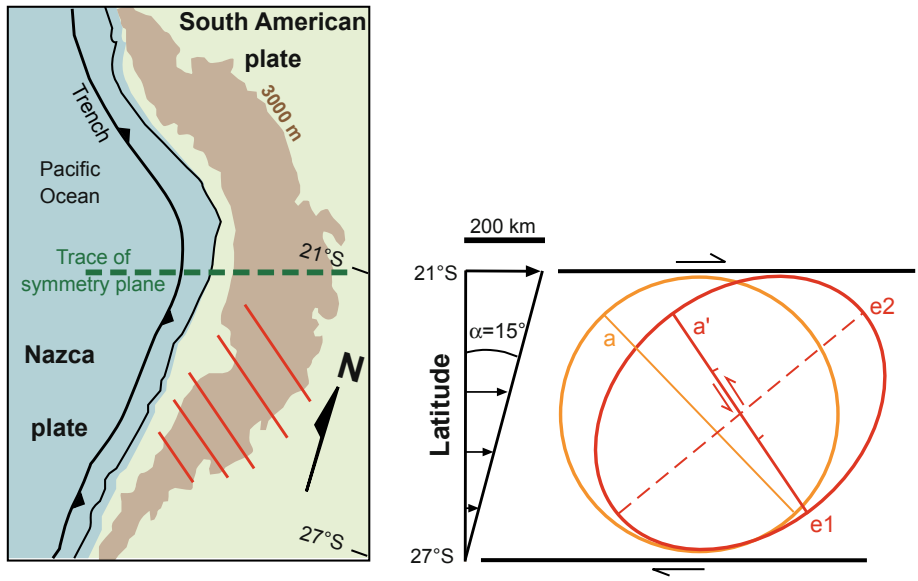

Fig. 12.21 Origin of transverse structures in the Central Andes. Left: bilateral symmetry of the Central Andes. The shaded area is higher than 3 km above sea level. NW–SE striking red lines delineate the traces of major fault zones associated with the transverse volcanic zones. Right: the horizontal sectional strain ellipse, explaining the NW–SE transtensive structures, is deduced from the gradient in transverse shortening in the southern portion of the Central Andes (modified after Riller et al. 2001)

lineaments identified from remote sensing and field analysis (Matteini et al. 2002; Trumbull et al. 2006). These belts are first-order fault zones of the Altiplano-Puna plateau, whose formation and left-lateral transtensive motion results from the gradient in transverse shortening from the central part of the plateau to its southern extent (Fig. 12.21). In addition, there appears to be a local control of pre-existing upper crustal weaknesses, with different orientation and kinematics, on the distribution and activity of polygenic and monogenic volcanoes (Riller et al. 2001; Acocella et al. 2011; Tibaldi et al. 2017).

The largest and best-studied transverse lineament is the ~300 km long Calama-Olacapato-El Toro fault zone. It consists of ~21 major magmatic centres, including explosive vents, calderas, composite stratovolcanoes, monogenetic cones, lava domes and plutons, active since Miocene. The Neogene left-lateral displacement of the Calama-Olacapato-El Toro fault zone is estimated as of ~20 km; in addition, the fault zone is associated with N-S trending extension (Fig. 12.22; Schurr et al. 1999; Riller et al. 2001). Overall left-lateral transtension has facilitated the ascent of magma and caldera formation. The SiO_2 content and $^{87}Sr/^{86}Sr$ ratio of the magmatic rocks suggest that the most evolved products, with upper crustal imprint, focus on the more intensively deformed central fault zone. Conversely, the more primitive, mantle-derived mafic to moderately evolved products focus toward the termini. This points to a genetic relationship between upper-crustal deformation and magmatic activity, leading to encouraged magma storage in the central fault zone (Riller et al. 2001; Petrinovic et al. 2006; Acocella et al. 2011).

12.5 A Synthetic Model for Convergent Plate Boundaries

As presented above, the structural control on arc volcanoes may vary significantly, involving extensional, strike-slip, contractional and oblique systems. The overall structure of the arc is highly

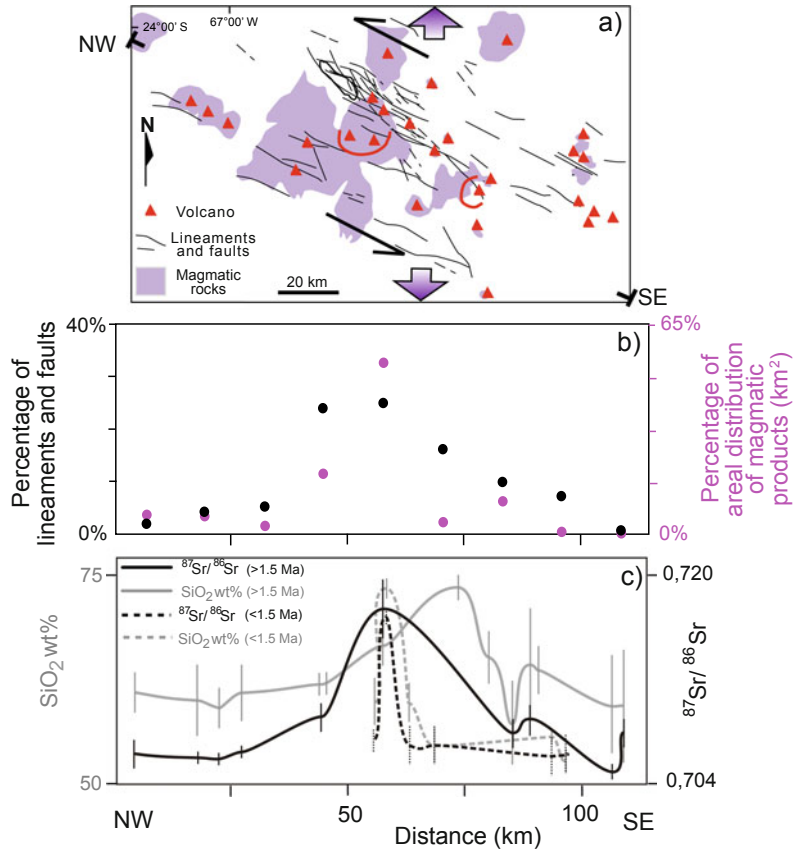

Fig. 12.22 Main tectono-magmatic features of the central and eastern part of the Calama-Olacapato-El Toro (COT) fault zone (location in Fig. 12.19; modified after Acocella et al. 2011). **a** Location of the main volcanoes (triangles), extent of magmatic rocks (in purple), main lineaments and faults (undistinguished). The overall kinematics of the fault zone consists of left-lateral transtension with orogen-parallel extension. **b** Percentages of the lineaments and faults (black) and of the areal distribution of the magmatic products (purple, in km^2) projected as a function of distance along the COT fault zone (see trace of profile in **a**). **c** SiO_2 wt% and $^{87}Sr/^{86}Sr$ ratio of the magmatic products as a function of distance from arc, highlighting more evolved compositions in the most fractured central part of the COT; vertical lines = range of values for each magmatic centre

dependent upon its tectonic setting, as imposed by relative plate motion (Table 12.2). A strike-slip motion along the arc results from a non-negligible trench-parallel component between the converging plates, whereas a dip-slip motion, responsible for extension or contraction, depends on the dominant trench-normal convergence (or subduction) velocity. Extensional conditions along the arc are usually associated with the highest magmatic output (as in the Taupo Volcanic Zone). However, the magmatic output can be important also in contractional arcs, as magma generation above slabs is a steady process. Indeed, contractional arcs may be associated with shallow magma accumulation via stacked sills capable of increasing the vertical stress component, ultimately producing significant volcanism, as in northeast Honshu. Following specific processes (slab steepening and lithospheric delamination, as in the Central Andes) contractional arcs may even produce exceptional amounts of magma.

The type and composition of arc volcanoes are broadly related to their structural setting. While calderas are usually related to felsic (rhyolite) compositions, stratovolcanoes are

Table 12.2 Summary of the relations between the tectonic setting, the structure of the volcanic arc and the amount of erupted magma along the arc (modified after Acocella and Funiciello 2010)

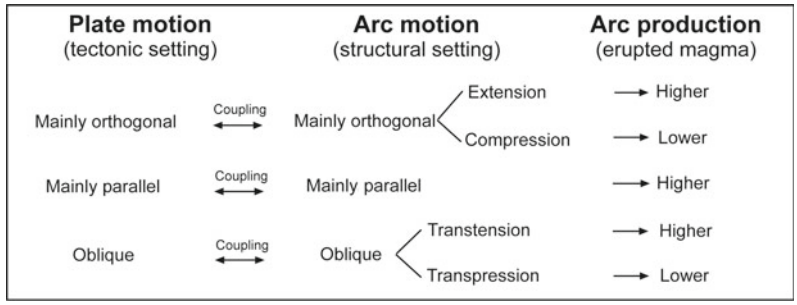

associated with intermediate (andesite) compositions. Also, while calderas predominate in highly productive and extensional arcs (as TVZ and the Tyrrhenian margin), stratovolcanoes are more frequent in poorly extending (Cascades), strike-slip (Sumatra) and contractional arcs (northeast Honshu). This suggests that arc extension is a requisite to develop the large and long-lived rhyolitic reservoirs below felsic calderas. The Central Andes show a distinct behaviour, as hosting large felsic calderas in an overall contractional arc. Their extremely high eruption rate is roughly equivalent to that of the extensional TVZ, albeit lasting much longer (Houghton et al. 1995). This indicates that in a contractional setting a sequence of external regional conditions (promoting slab steepening and lithospheric delamination), can be equally effective as sustained extension in producing significant volumes of arc volcanism.

The structure of a volcanic arc is not necessarily continuous, with a first-order tectono-magmatic segmentation evident in the distribution of the surface deformation and of monogenic and polygenic volcanoes, as well as their output rates. This segmentation may result from regional stress gradients, associated with microplates, forearc slivers and torn slabs. At a more local scale, the segmentation may also result from the presence of any magmatic system, defined by the continuation of magmatic activity outside a main polygenic volcano, suggesting enhanced conditions for the shallow intrusion of magma. Magmatic systems show a variability depending on the structural setting. Volcanic arcs undergoing evident extension, as TVZ, show a similar architecture to that of mature continental divergent plate boundaries. In fact, volcanic and tectonic activity in both settings is segmented and focused in magmatic systems with similar extension rate and geometry. Major rifting episodes may result from the emplacement of kilometres long mafic dikes, as during the 1886 Tarawera eruption in TVZ or in the early nineteenth century in the northern Main Ethiopian Rift. A small-scale example of volcanic arc experiencing dominant extension and similarly associated with magmatic systems is the Central Aeolian Arc (Italy). Here extension occurs at shallow crustal levels and appears magma-induced, while strike-slip structures are probably active at deeper levels (Ruch et al. 2016). Magmatic systems in volcanic arcs experiencing minor extension (≤ 0.1 cm/year; as the Cascades, Izu-Bonin or the Trans-Mexican Volcanic Belt, Mexico) are less developed or not evident. For example, in 2000 a tens of kilometres long dike propagated laterally out of Miyakejima Island, in the weakly extending Izu-Bonin Arc, suggesting that magmatic activity continues outside the central volcano, although the direction of propagation was subparallel to the direction of convergence (Toda et al. 2002). These features suggest that an extension rate of a few mm/year marks the threshold between arcs with magmatic systems, structurally similar to

continental divergent plate boundaries, and arcs with poor or no evidence of magmatic systems. In any case, the structure of extensional arcs is complicated by the fact that the volcanic segmentation, as related to the arc-normal tension, may also result from the stress regime related to the changing dip of the slab and the breadth of the zone coupling with the overriding plate, as highlighted for the Marianas (Andikagumi et al. 2020). Arcs undergoing predominant strike-slip motion also lack evident or recurrent magmatic systems. In the South Andean Volcanic Zone, a few volcanic complexes (as Puyehue–Cordón Caulle, Nevados de Chillan and Laguna del Maule) may resemble magmatic systems, although most polygenic volcanoes lack evidence of volcanic activity continuing outside the edifice. In Sumatra, magmatic systems are lacking and volcanic activity remains, with the exception of Toba caldera, largely punctiform or central. Arc volcanoes undergoing contraction elongate and align parallel to the direction of maximum principal stress σ_1, as in northeast Honshu. Here the Quaternary arc-orthogonal alignment and elongation of volcanoes mimics the direction of "hot mantle fingers" at the sublithospheric scale. However, being volcanic activity restricted to the polygenic volcano, there is no evidence of magmatic systems. Therefore, the linear mode of magmatic accretion of divergent plate boundaries and, partly, extensional arcs is gradually replaced by a dominant central mode of accretion in strike-slip arcs, where magmatic systems are very limited, and an exclusively central mode in contractional arcs, where magmatic systems are absent (Acocella 2014). The Central Andes provide a distinct behaviour, as, for their specific evolution, the predominant central mode of magmatic accretion feeds areal volcanism.

The general transition from linear to central magmatic accretion may be partly reconciled with the average depth of the magma plumbing systems below polygenic arc volcanoes (Fig. 12.23; e.g., Chaussard and Amelung 2012). In fact, the development of a magmatic system, being promoted by shallower magma chambers and dike swarms, depends also upon the average depth of its magma plumbing system. In arc volcanoes, this depth depends upon the arc structure. Arcs undergoing extension and strike-slip motion usually have shallower magma

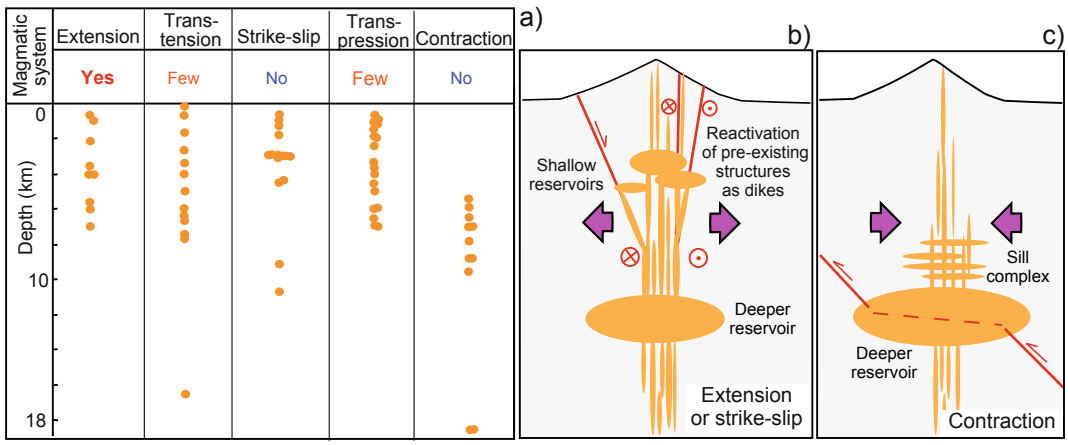

Fig. 12.23 **a** Degree of development of magmatic systems (above) and depths of magma reservoirs as a function of the stress regime in extensional, transtensive, strike-slip, transpressive and contractional volcanic arcs. Reservoir depths are from geodesy, seismology, gravity or petrology. Stress regime is from seismic Centroid Moment Tensor data (CMT) and World Stress Map Project data. **b** and **c** Interpretative cartoons showing in section view the effect of the tectonic setting on magma ascent through the upper crust in volcanic arcs. Extensional and strike-slip settings promote shallow level reservoirs and dikes, while contractional settings promote intermediate-level sills (modified after Chaussard and Amelung 2012)

reservoirs and dike systems, whereas arcs undergoing contraction have deeper reservoirs and dike systems. These structural conditions determine different possibilities for magma to accumulate at shallow crustal levels, propagate vertically and laterally and rise towards the surface, ultimately developing a magmatic system. Therefore, the lack of magmatic systems in contractional arcs may be explained by their deeper magma plumbing systems, which impose a more focused (central) volcanic activity.

Similarly to divergent plate boundaries, magma also affects the evolution of convergent plate boundaries: this may occur through very different mechanisms, which depend on the arc structure. The tectono-magmatic behaviour of some extensional arcs (TVZ) resembles that of continental divergent plate boundaries, where dikes promote shallow opening and magma assists rifting at depth. At the extreme, magma-induced extension may even mask surface evidence of strike-slip structures active in the arc roots, as in the Central Aeolian Arc. In addition, in several arcs the emplacement of magma at depth determines the thermal weakening of the crust, localizing the shallow deformation. This occurs in extensional arcs (Taupo Volcanic Zone) and in strike-slip arcs (Sumatra and South Andean Volcanic Zone), where the fault zones coincide with the core of the volcanic arc (Kendall et al. 2005; Ruch et al. 2016; Villamor et al. 2017; Acocella et al. 2018; Gase et al. 2019). In some arcs with strike-slip component (Kuril Arc and Trans Mexican Volcanic Belt), the weakening may induce an effective decoupling between forearc and back-arc, developing a forearc sliver. Nevertheless, under certain conditions the high thermal state of the crust may locally inhibit faulting: for example, propagating regional faults and related seismicity repeatedly arrested in correspondence of magma chambers, as observed in 1994 after the Liwa earthquake (southern Sumatra) and in 2016 at Aso caldera (western Japan; Widiwijayanti et al. 1996; Lin et al. 2016).

While in obliquely-convergent arcs magma may focus crustal deformation, the produced strike-slip zone may in turn influence magmatic and volcanic activity. In fact, studies on the plutons constituting the roots of eroded volcanic arcs show that pluton growth is promoted by oblique convergence conditions, when strain partitioning activates strike-slip faults creating localised extensional zones, as pull-apart structures, releasing bends and dilational jogs able to promote the rise, emplacement and accumulation of magma (see Fig. 4.20). Similar processes are expected to promote the rise and emplacement of magma and assist the development of magma chambers also below the active volcanoes of Sumatra or the South Andean Volcanic Zone. This may lead to a feedback between magmatic activity and strike-slip faulting along volcanic arcs, where the former localizes the site of active deformation and the latter assists the development of the magma reservoirs constituting the roots of the arcs. Nevertheless, at the surface the control of strike-slip structures on the location and activity of the volcanoes is less evident, as observed at Sumatra or the South Andean Volcanic Zone. In fact, in both cases the location of only a part of the volcanoes may be related to the activity of the strike-slip structures, with another part simply compliant with the responsible regional stress field. Despite the working hypothesis presented in Sect. 12.3.2 of a variable role of the arc structure at depth and at the surface, the limited agreement between these deeper and shallower tectono-magmatic relationships along strike-slip arcs remains poorly understood.

Contractional arcs also show an active role of magma, at times assisted by regional tectonics. In northeast Honshu, pressurized stacked sills may locally increase the vertical component of the principal stress from σ_3 to σ_2 and even to σ_1, promoting arc-parallel extension and arc-perpendicular alignment and elongation of volcanoes. In addition, the co- and post-seismic deformation induced by mega-earthquakes may induce transient stress variations, promoting extension in contractional and strike-slip arcs. This may enhance diking, gas nucleation, magma mixing and ultimately the rise of magma, increasing the eruptive frequency in the post-seismic period. In this case, assisted by regional tectonics, dikes may also intrude and feed

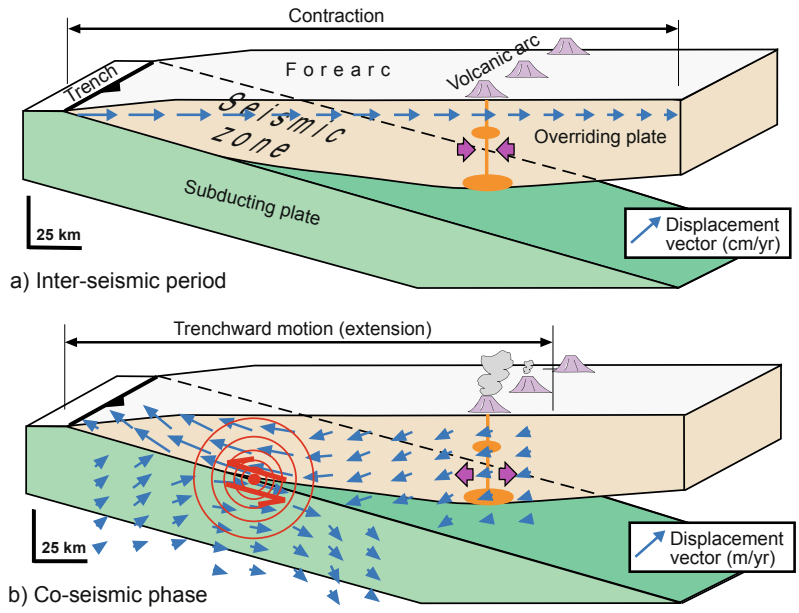

Fig. 12.24 **a** Schematic cross section of a subduction zone in the inter-seismic period, where the overall compressive stress field generates progressively decreasing displacement vectors (blue arrows) pointing towards the inner part of the overriding plate. The volcanoes and their plumbing systems (in orange) experience contraction (purple arrows). **b** Cross section of a subduction zone in the co-seismic phase. The co-seismic displacement field (blue arrows) associated with a megathrust earthquake (red arrows) induces a trenchward movement of the overriding plate. This kinematic inversion extends this portion of the upper plate, promoting volumetric expansion (purple arrows) in the plumbing systems of the volcanoes (orange; modified after Walter and Amelung 2007)

volcanic activity along otherwise non-favourable orientations, as parallel to the arc (northeast Honshu) or perpendicular to the oblique convergence vector (southern Andes; Fig. 12.24; Walter and Amelung 2007; Jonsson 2013).

These different cases from extensional, strike-slip and contractional arcs indicate that magma-driven variations in the stress state or in the structure of a volcanic arc are feasible and common. Therefore, magma may play a dominant role in controlling the evolution of convergent plate boundaries through diking, sill stacking, heat-induced strain localization and stress transients. This implies that a significant part of the structure of a volcanic arc may be magma-induced or assisted, with magmatic processes being largely self-sustained and requiring limited external tectonic contribution.

12.6 Summary

Arc volcanoes may be controlled by extensional, strike-slip, contractional or oblique structures, depending upon the tectonic setting imposed by the converging plates. In particular, the structure of the arc determines the distribution of its volcanism and ultimately the presence and development of the magmatic systems. Arcs experiencing evident extension (several mm/yr, as TVZ) have magmatic systems similar to those of mature continental divergent plate boundaries. Arcs experiencing strike-slip motion (as the South Andean Volcanic Zone or Sumatra) lack dominant magmatic systems, although these may be locally identified. Contractional arcs (as northeast Honshu) lack any evidence of

magmatic systems. Therefore, the linear mode of magmatic accretion of divergent plate boundaries and extending arcs is replaced by a dominant central mode of accretion in strike-slip arcs and a completely central mode in contractional arcs. This feature may be a consequence of the shallower magma plumbing systems in volcanic arcs experiencing extension. A distinct behaviour is observed in the contractional arc of the Central Andes, characterized by an areal mode of magmatic accretion resulting from its exceptional productivity.

The structure of a volcanic arc in turn also determines the dominant mechanism(s) through which magma affects the evolution of the convergent plate boundary. These mechanisms include diking, sill stacking, heat-induced weakening and transient stresses induced by mega-earthquakes, suggesting that a significant part of the development of a volcanic arc is magma-induced, with magmatic processes being largely self-sustained, though not insensitive to regional tectonics.

References

Acocella V, Funiciello R (2006) Transverse systems along the extensional Tyrrhenian margin of central Italy and their influence on volcanism. Tectonics 25: TC2003. https://doi.org/10.1029/2005TC001845

Acocella V, Spinks K, Cole J, Nicol A (2003) Oblique back-arc rifting of Taupo Volcanic Zone, New Zealand. Tectonics 22:1045. https://doi.org/10.1029/2002TC001447

Acocella V, Yoshida T, Yamada R, Funiciello F (2008) Structural control on late miocene to quaternary volcanism in the NE Honshu arc, Japan. Tectonics 27:TC5008. https://doi.org/10.1029/2008TC002296

Acocella V, Funiciello F (2010) Kinematic setting and structural control of arc volcanism. Earth Planet Sci Lett 289:43–53

Acocella V, Gioncada A, Omarini R, Riller U, Mazzuoli R, Vezzoli L (2011) Tectono-magmatic characteristics of the eastern Calama-Olacapato-El Toro lineament, Central Andes. Tectonics 30:TC3005. https://doi.org/10.1029/2010TC002854

Acocella V (2014) Structural control on magmatism along divergent and convergent plate boundaries: overview, model, problems. Earth-Sci Rev 136:226–288

Acocella V, Bellier O, Sandri L, Sébrier M, Pramumijoyo S (2018) Weak tectono-magmatic relationships along an obliquely convergent plate boundary: Sumatra, Indonesia. Front Earth Sci 6:3. https://doi.org/10.3389/feart.2018.00003

Allan ASR, Wilson CJN, Millet MA, Wysoczansk RJ (2012) The invisible hand: tectonic triggering and modulation of a rhyolitic supereruption. Geology 40:563–566

Allmendinger RW, Gubbels T (1996) Pure and simple shear plateau uplift, Altiplano-Puna, Argentina and Bolivia. Tectonophysics 259:1–13

Allmendinger RW, Jordan TE, Kay SM, Isacks BL (1997) The evolution of the Altiplano-Puna Plateau of the Central Andes. Annu Rev Earth Planet Sci 25:139–174

ANCORP Working Group (2003) Seismic imaging of a convergent continental margin and plateau in the central Andes (Andean Continental Research Project 1996 (ANCORP'96)). J Geophys Res 108:2328. https://doi.org/10.1029/2002JB001771

Andikagumi H, Macpherson CG, McCaffrey KJW (2020) Upper plate stress controls the distribution o Mariana Arc volcanoes. J Geophys Res 125:e2019JB017391. https://doi.org/10.1029/2019JB017391

Barberi F, Buonasorte G, Cioni R, Fiordelisi A, Foresi L, Iaccarino S et al (1994) Plio-pleistocene geological evolution of the geothermal area of tuscany and latium. Mem Descr Carta Geol Ital XLIX:77–134

Barker SJ, Wilson CJN, Morgan DJ, Rowland JV (2016) Rapid priming, accumulation, and recharge of magma driving recent eruptions at a hyperactive caldera volcano. Geology 44:323–326

Begg JG, Mouslopoulou V (2010) Analysis of late Holocene faulting within an active rift using lidar, Taupo Rift, New Zealand. J Volcanol Geoth Res 190:152–167

Bellier O, Bellon H, Sebrier M, Sutanto P, Maury RC (1999) K-Ar age of the Ranau tuffs: implications for the Ranau caldera emplacement and slip-partitioning in Sumatra (Indonesia). Tectonophysics 312:347–359

Benoit MH, Torpey M, Liszewski K, Levin V, Park J (2011) P and S wave upper mantle seismic velocity structure beneath the northern Apennines: New evidence for the end of subduction. Geochem Geophys Geosyst 12:Q06004. https://doi.org/10.1029/2010GC003428

Bertrand EA, Caldwell TG, Hill GJ, Wallin EL, Bennier SL, Cozens N et al (2012) Magnetotelluric imaging of upper-crustal convection plumes beneath the Taupo Volcanic Zone, New Zealand. Geophys Res Lett 39:L02304. https://doi.org/10.1029/2011GL050177

Best MG, Christiansen EH, de Silva S, Lipman PW (2016) Slab-rollback ignimbrite flareups in the southern Great Basin and other Cenozoic American arcs: a distinct style of arc volcanism. Geosphere 12:1097–1135

Bianchi M, Heit B, Jakovlev A, Yuan X, Kay SM, Sandvol E et al (2013) Teleseismic tomography of the southern Puna plateau in Argentina and adjacent regions. Tectonophysics 586:65–83

Blakely RJ, Christiansen RL, Guffanti M, Wells RE, Donnelly-Nolan JM, Muffler LJP et al (1997) Gravity anomalies, Quaternary vents, and Quaternary faults in the southern Cascade Range, Oregon and California: implications for arc and backarc evolution. J Geophys Res 102:22513–22527

Bonali FL, Tibaldi A, Corazzato C (2015) Sensitivity analysis of earthquake-induced static stress changes on volcanoes: the 2010 Mw 8.8 Chile earthquake. Geophys J Int 201:1868–1890

Bradley KE, Feng L, Hill EM, Natawidjaja DH, Sieh K (2017) Implications of the diffuse deformation of the Indian Ocean lithosphere for slip partitioning of oblique plate convergence in Sumatra. J Geophys Res 122:572–591

Bucchi F, Lara LE, Gutierrez F (2015) The Carrán-Los Venados volcanic field and its relationship with coeval and nearby polygenetic volcanism in an intra-arc setting. J Volcanol Geoth Res 308:70–81

Caratori Tontini F, Bassett D, de Ronde CEJ, Timm J, Wysoczanski R (2019) Early evolution of a young back-arc basin in the Havre Trough. Nat Geosci 12:856–862

Cembrano J, Lara L (2009) The link between volcanism and tectonics in the southern volcanic zone of the Chilean Andes: a review. Tectonophysics 471:96–113

Chaussard E, Amelung F (2012) Precursory inflation of shallow magma reservoirs at west Sunda volcanoes detected by InSAR. Geophys Res Lett 39:L21311. https://doi.org/10.1029/2012GL053817

Chesner CA (2012) The Toba Caldera Complex. Quatern Int 258:5–18

Cladouhos IT, Allmendinger RW, Coira B, Farrar E (1994) Late Cenozoic deformations in the Central Andes: fault kinematics from the northern Puna, northwest Argentina and southwest Bolivia. J South Am Earth Sci 7:209–228

Cole JW (1990) Structural control and origin of volcanism in the Taupo Volcanic Zone, New Zealand. Bull Volcanol 52:445–459

Coutand I, Cobbold PR, de Urreiztieta M, Gautier P, Chauvin A, Gapais D et al (2001) Style and history of Andean deformation, Puna plateau, northwestern Argentina. Tectonics 20:210–234

D'Agostino N (2014) Complete seismic release of tectonic strain and earthquake recurrence in the Apennines (Italy). Geophys Res Lett 41. https://doi.org/10.1002/2014GL059230

Darby DJ, Meertens CM (1995) Terrestrial and GPS measurements of deformation across the Taupo back arc and Hikurangi forearc regions in New Zealand. J Geophys Res 100:8221–8232

De Maisonneuve CB, Dungan MA, Bachmann O, Burgisser A (2012) Insights into shallow magma storage and crystallization at Volcán Llaima (Andean Southern Volcanic Zone, Chile). J Volcanol Geoth Res 211:76–91

DeMets C (1992) Oblique convergence and deformation along the Kuril and Japanese trenches. J Geophys Res 97:17615–17625

DeMets C, Traylen S (2000) Motion of the Rivera plate since 10 Ma relative to the Pacific and North American plates and the mantle. Tectonophysics 318:119–159

de Silva SL, Gosnold WD (2007) Episodic construction of batholiths: insights from the spatiotemporal development of an ignimbrite flare-up. J Volcanol Geoth Res 167:320–335

de Silva SK, Kay SM (2018) Turning up the heat: high-flux magmatism in the Central Andes. Elements 14:245–250

de Silva SL, Mucek AE, Gregg PM, Pratomo I (2015) Resurgent Toba-field, chronologic, and model constraints on duration, time scales and mechanisms of resurgence at large calderas. Front Earth Sci 3. https://doi.org/10.3389/feart.2015.00025

Deering CD, Cole JW, Vogel TA (2008) Rhyolite compositional continuum governed by lower crustal source conditions in the Taupo Volcanic Zone, New Zealand. J Petrol 49:2245–2276

Delgado F, Pritchard ME, Basualto D, Lazo J, Córdova L, Lara LE (2016) Rapid reinflation following the 2011–2012 rhyodacite eruption at Cordón Caulle volcano (Southern Andes) imaged by InSAR: Evidence for magma reservoir refill. Geophys Res Lett 43:9552–9562

Delgado F, Kubanek J, Anderson K, Lundgren P, Pritchard M (2019) Physicochemical models of effusive rhyolitic eruptions constrained with InSAR and DEM data: A case study of the 2011–2012 Cordón Caulle eruption). Earth Planet Sci Lett 524:115736

Detourbet C, Bellier O, Sébrier M (1993) La caldeira volcanique de Toba et la Grande Faille de Sumatra (Indonesie) vues par l'imagerie SPOT. CR Acad Sci Paris 316:1439–1445

Devoti R, Esposito A, Pietrantonio G, Pisani AR, Riguzzi F (2011) Evidence of large scale deformation patterns from GPS data in the Italian subduction boundary. Earth Planet Sci Lett 311:230–241

Di Luccio F, Chiodini G, Caliro S, Cardellini C, Convertito V, Pino NA (2018) Seismic signature of active intrusions in mountain chains. Sci Adv 4:e1701825

Di Stefano R, Bianchi I, Ciaccio MG, Carrara G, Kissling E (2011) Three-dimensional Moho topography in Italy: New constraints from receiver functions and controlled source seismology. Geochem Geophys Geosyst 12:Q09006. https://doi.org/10.1029/2011GC003649

Duquesnoy TH, Bellier O, Kasser M, Sébrier M, Vigny CH, Bahar I (1996) Deformation related to the 1994 Liwa earthquake derived from geodetic measurements. Geophys Res Lett 23:3055–3058

Eberhart-Phillips D, Bannister S, Reyners M (2020) Attenuation in the mantle wedge beneath supervolcanoes of the Taupo Volcanic Zone, New Zealand. Geophys J Int 220:703–723

Faccenna C, Funiciello R, Bruni A, Mattei M, Sagnotti L (1994) Evolution of a transfer related basin: the Ardea basin (Latium, Central Italy). Basin Res 6:35–46

Flinders AF, Shen Y (2017) Seismic evidence for a possible deep crustal hot zone beneath Southwest Washington. Sci Rep 7:7400. https://doi.org/10.1038/s41598-017-07123-w

Folguera A, Ramos VA, Hermanns RL, Naranjo J (2004) Neotectonics in the foothills of the southernmost central Andes (37–38 S): evidence of strike-slip displacement along the Antiñir-Copahue fault zone. Tectonics 23: TC5008. https://doi.org/10.1029/2003TC001533

Gahalaut VK, Jade S, Catherine JK, Gireedh R, Ananda MB, Dileep Kumar P et al (2008) GPS measurements of postseismic deformation in the Andaman-Nicobar region following the giant 2004 Sumatra-Andaman earthquake. J Geophys Res 113: B08401. https://doi.org/10.1029/2007JB005511

Galland O, Hallot E, Cobbold PR, Ruffet G, de Bremond d'Ars J (2007) Volcanism in a compressional Andean setting: a structural and geochronology study of Tromen volcano (Neuquen province, Argentina). Tectonics 26: TC4010. https://doi.org/10.1029/2006TC002011

Gao H, Humphreys E, Yao H, van der Hilst RD (2011) Crust and lithosphere structure of the northwestern U. S. with ambient noise tomography: Terrane accretion and Cascade arc development. Earth Planet Sci Lett 304:202–211

Gase AC, Van Avendonk HJA, Bangs NL, Luckie TW, Barker DHN, Henrys SA et al (2019) Seismic evidence of magmatic rifting in the offshore Taupo Volcanic Zone, New Zealand. Geophys Res Lett 46:12949–12957

Gasparon M (2005) Quaternary volcanicity. In: Barber AJ, Crow ML, Milsom JS (eds) Sumatra: geology, resources and tectonic evolution. Geol Soc London Memoir London UK 31:120–130

Genrich JF, Bock Y, McCaffrey R, Prawirodirdjo L, Stevens CW, Puntodewo SSO et al (2000) Distribution of slip at the northern Sumatran fault system. J Geophys Res 105:28327–28341

George OA, Malservisi R, Govers R, Connor CB, Connor LJ (2016) Is uplift of volcano clusters in the Tohoku Volcanic Arc, Japan, driven by magma accumulation in hot zones? A geodynamic modeling study. J Geophys Res 121:4780–4796

Giacomuzzi G, Civalleri M, De Gori P, Chiarabba C (2012) A 3D Vs model of the upper mantle beneath Italy: Insight on the geodynamics of central Mediterranean. Earth Planet Sci Lett 335–336:105–120

Gioncada A, Vezzoli L, Mazzuoli R, Omarini R, Nonnotte P, Guillou H (2010) Pliocene intraplate-type volcanism in the Andean foreland at 26°10′S, 64°40′ W (NW Argentina): Implications for magmatic and structural evolution of the Central Andes. Lithosphere 2:153–171

Gomez-Vasconcelos MG, Villamor P, Cronin S, Procter J, Palmer A, Townsend D et al (2017) Crustal extension in the Tongariro graben, New Zealand: insights into volcano-tectonic interactions and active deformation in a young continental rift. Geol Soc Am Bull 129:1085–1099

Gonzalez G, Cembrano J, Aron F, Veloso EE, Shyu JBH (2009) Coeval compressional deformation and volcanism in the central Andes, case studies from northern Chile (23°S-24°S). Tectonics 28:TC6003. https://doi.org/10.1029/2009TC002538

Gravley DM, Wilson CJN, Leonard GS, Cole JW (2007) Double trouble: paired ignimbrite eruptions and collateral subsidence in the Taupo Volcanic Zone, New Zealand. Geol Soc Am Bull 119:18–30

Gravley DM, Deering CD, Leonard GS, Rowland JV (2016) Ignimbrite flare-ups and their drivers: A New Zealand perspective. Earth Sci Rev 162:65–82

Green NL, Harry DL (1999) On the relationship between subducted slab age and arc basalt petrogenesis, Cascadia subduction system, North America. Earth Planet Sci Lett 171:367–381

Gripp AE, Gordon RG (2002) Young tracks of hotspots and current plate velocities. Geophys J Int 150:321–361

Grocott J, Brown M, Dallmeyer RD, Taylor GK, Treloar PJ (1994) Mechanisms of continental growth in extensional arcs: an example from the Andean plate-boundary zone. Geology 22:391–394

Guffanti M, Weaver CS (1988) Distribution of Late Cenozoic Volcanic Vents in the Cascade Range's Volcanic Arc Segmentation and Regional Tectonic Considerations. J Geophys Res 93:6513–6529

Gurer D, Galland O, Corfu F, Leanza HA, Sassier C (2016) Structure and evolution of volcanic plumbing systems in fold-and-thrust belts: A case study of the Cerro Negro de Tricao Malal, Neuquén Province, Argentina. Geol Soc Am Bull 128:315–331

Hamling IJ, Hreinsdottir S, Fournier N (2015) The ups and downs of the TVZ: geodetic observations of deformation around the Taupo Volcanic Zone, New Zealand. J Geophys Res 120:4667–4679

Hamling IJ, Hreinsdóttir S, Bannister S, Palmer N (2016) Off-axis magmatism along a subaerial back-arc rift: observations from the Taupo Volcanic Zone, New Zealand. Sci Adv 2:e1600288

Hasegawa A, Zhao D, Hori S, Yamamoto A, Horiuchi S (1991) Deep structure of the northeastern Japan arc and its relationship to seismic and volcanic activity. Nature 352:683–689

Heise W, Bibby HM, Caldwell TG, Nanninster SC, Ogawa Y, Takakura S et al (2007) Melt distribution beneath a young continental rift: the Taupo Volcanic Zone, New Zealand. Geophys Res Lett 34:L14313. https://doi.org/10.1029/2007GL029629

Hildreth W (2007) Quaternary magmatism in the Cascades; geologic perspectives. US Geological Survey Professional Paper 1744,125 p

Hindle D, Kley J, Oncken O, Sobolev S (2005) Crustal balance and crustal flux from shortening estimates in the Central Andes. Earth Planet Sci Lett 230:113–124

Holden L, Wallace L, Beavan J, Fournier N, Cas R, Ailleres L et al (2015) Contemporary ground deformation in the Taupo Rift and Okataina Volcanic Centre from 1998 to 2011, measured using GPS. Geophys J Int 202:2082–2105

Houghton BF, Wilson CJN, McWilliams MO, Lanphere MA, Weaver SD, Briggs RM et al (1995) Chronology and dynamics of a large silicic magmatic system: central Taupo Volcanic Zone, New Zealand. Geology 23:13–16

Houlie N, Stern TA (2017) Vertical tectonics at an active continental margin. Earth Planet Sci Lett 457:292–301

Igarashi T, Matsuzawa T, Umino N, Hasegawa A (2001) Spatial distribution of focal mechanisms for interplate and intraplate earthquakes associated with the subducting plate beneath the northeastern Japan arc: a triple-planned deep seismic zone. J Geophys Res 106:2177–2191

Ito T, Yoshioka S, Miyazaki S (2000) Interplate coupling in northeast Japan deduced from inversion analysis of GPS data. Earth Planet Sci Lett 176:117–130

Ito T, Gunawan E, Kimata F, Tabei T, Meilano I, Agustan et al (2016) Co-seismic offsets due to two earthquakes (Mw 6.1) along the Sumatran fault system derived from GNSS measurements. Earth Planets Space 68:57. https://doi.org/10.1186/s40623-016-0427-z

Jaxybulatov K, Shapiro NM, Koulakov I, Mordret A, Landes M, Sens-Schönfelder C (2014) A large magmatic sill complex beneath the Toba caldera. Science 346:617–619

Jay J, Costa F, Pritchard M, Lara L, Singer B, Herrin J (2014) Locating magma reservoirs using InSAR and petrology before and during the 2011–2012 Cordón Caulle silicic eruption. Earth Planet Sci Lett 395:254–266

Jolivet L, Faccenna C, Goffé B, Mattei M, Rossetti F, Brunet C et al (1998) Midcrustal shear zones in postorogenic extension: example from the northern Tyrrhenian Sea. J Geophys Res 103:12123–12160

JJonsson S (2013) Sunken volcanoes. Nat Geosci 6:891–892

Jordan TE, Isacks BL, Allmendinger RW, Brewer JA, Ramos VA, Ando CJ (1983) Andean tectonics related to geometry of subducted Nazca plate. Geol Soc Am Bull 94:341–361

Kato N, Sato H, Umino N (2006) Fault reactivation and active tectonics on the fore-arc side of the back-arc rift system, NE Japan. J Struct Geol 28:2011–2022

Kay SM, Coira BL (2009) Shallowing and steepening subduction zones, continental lithospheric loss, magmatism, and crustal flow under the central Andean Altiplano-Puna Plateau. In: Kay SM, Ramos VA, Dickinson WR (eds) Backbone of the Americas: shallow subduction, plateau uplift, and ridge and terrane collision. Geol Soc Am Memoir 204:229–260

Kay RW, Kay SM (1993) Delamination and delamination magmatism. Tectonophysics 219:177–189

Kendall JM, Stuart GW, Ebinger CJ, Bastow ID, Keir D (2005) Magma-assisted rifting in Ethiopia. Nature 433:146–148

Kimura G (1986) Oblique subduction and collision: forearc tectonics of the Kuril arc. Geology 14:404–407

Kimura G (1996) Collision orogeny at arc-arc junctions in the Japanese Islands. The Island Arc 5:262–275

Koulakov I, Kasatkina E, Shapiro NM, Jaupart C, Vasilevsky A, El Khrepy S et al (2016) The feeder system of the Toba supervolcano from the slab to the shallow reservoir. Nature Communications 7:12228. https://doi.org/10.1038/ncomms12228

Kundu B, Legrand D, Gahalaut K, Gahalaut VK, Mahesh P, Kamesh Raju KA et al (2012) The 2005 volcano-tectonic earthquake swarm in the Andaman Sea: triggered by the 2004 great Sumatra-Andaman earthquake. Tectonics 31:TC5009. https://doi.org/10.1029/2012TC003138

Lara LE, Naranjo JA, Moreno H (2004) Rhyodacitic fissure eruption in Southern Andes (Cordon Caulle; 40.5°S) after the 1960 (Mw:9.5) Chilean earthquake: a structural interpretation. J Volcanol Geoth Res 138:127–138

Lara LE, Moreno H, Naranjo JA, Matthews S, Perez de Arce C (2006) Magmatic evolution of the Puyehue-Cordón Caulle Volcanic Complex (40°S), Southern Andean Volcanic Zone: From shield to unusual rhyolitic fissure volcanism. J Volcanol Geoth Res 157:343–366

Lara LE, Cembrano J, Lavenu BA (2010) Quaternary vertical displacement along the Liquiñe-Ofqui Fault Zone: differential uplift and coeval volcanism in the Southern Andes? Int Geol Rev 50:975–993

Lau N, Tymofyeyeva E, Fialko Y (2018) Earth Planet Sci Lett 491:43–47

Lavenu A, Cembrano J (1999) Compressional- and transpressional-stress pattern for Pliocene and Quaternary brittle deformation in fore arc and intra-arc zones (Andes of central and Southern Chile). J Struct Geol 21:1669–1691

Legrand D, Barrientos S, Bataille K, Cembrano J, Pavez A (2011) The fluid-driven tectonic swarm of Aysen Fjord, Chile (2007) associated with two earthquakes (Mw=6.1 and Mw=6.2) within the Liquine-Ofqui Fault Zone. Cont Shelf Res 31:154–161

Liang X, Sandvol E, Kay S, Heit B, Yuan X, Mulcahy P et al (2014) Delamination of southern Puna lithosphere revealed by body wave attenuation tomography. J Geophys Res 119:549–566

Lin A, Satsukawa T, Wang M, Mohammadi Asl Z, Fueta R, Nakajima F (2016) Coseismic rupturing stopped by Aso volcano during the 2016 Mw 7.1 Kumamoto earthquake, Japan. Science 354:869–874

Loveless JP, Meade BJ (2010) Geodetic imaging of plate motions, slip rates and partitioning of deformation in Japan. J Geophys Res 115:B02410. https://doi.org/10.1029/2008JB006248

Lupi M, Trippanera D, Gonzalez D, D'Amico S, Acocella V, Cabello C (2020) Megathrust earthquakes and the growth of NW-trending volcanic systems in the Southern Central Andes. Tectonophysics 774:228204

Mahony SH, Sparks RSJ, Wallace LM, Engwell SL, Scourse EM, Barnard NH et al (2016) Increased rates of large-magnitude explosive eruptions in Japan in the late Neogene and Quaternary. Geochem Geophys Geosyst 17:2467–2479

Malinverno A, Ryan WBF (1986) Extension in the Tyrrhenian Sea and shortening in the Apennines as

result of arc migration driven by sinking of the lithosphere. Tectonics 5:227–245
Mariani M, Prato R (1988) I bacini neogenici costieri del margine tirrenico: Approccio sismicostratigrafico. Mem Soc Geol Ital 41:519–531
Marra F, Taddeucci J, Freda C, Marzocchi W, Scarlato P (2004) Recurrence of volcanic activity along the Roman Comagmatic Province (Tyrrhenian margin of Italy) and its tectonic significance. Tectonics TC40n https://doi.org/10.1029/2003TC001600
Marrett R, Strecker MR (2000) Response of intracontinental deformation in the central Andes to the late Cenozoic reorganization of South American Plate motions. Tectonics 19:452–467
Matteini M, Mazzuoli R, Omarini R, Cas RAF, Maas R (2002) Geodynamical evolution of the Central Andes at 24°S as inferred by magma composition along the Calama–Olacapato–El Toro transversal volcanic belt. J Volcanol Geother Res 118:205–228
Mavrommatis AP, Segall P, Johnson KM (2014) A decadal-scale deformation transient prior to the 2011 Mw 9.0 Tohoku-Oki earthquake. Geophys Res Lett 41:4486–4494
McCaffrey R, Zwick PC, Bock Y, Prawirodirdjo L, Genrich JF, Stevens CW et al (2000) Strain partitioning during oblique plate convergence in northern Sumatra: geodetic and seismologic constraints and numerical modelling. J Geophys Res 105:28363–28376
McCaffrey R, Qamar AI, King RW, Wells R, Khazaradze G, Williams CA et al (2007) Fault locking, block rotation and crustal deformation in the Pacific Northwest. Geophys J Int 169:1315–1340
McCrory PA, Blair JL, Waldhauser F, Oppenheimer DH (2012) Juan de Fuca slab geometry and its relation to Wadati-Benioff zone seismicity. J Geophys Res 117: B09306. https://doi.org/10.1029/2012JB009407
McNulty B, Farber D, Wallace GS, Lopez R, Palacios O (1998) Role of plate kinematics and plate-slip-vector partitioning in continental magmatic arcs: evidence from the Cordillera Blanca, Peru. Geology 26:827–830
Melnick D, Folguera A, Ramos VA (2006) Structural control on arc volcanism: the caviahue-copahue complex, Central to Patagonian Andes transition (38°S). J S Am Earth Sci 22:66–88
Miller KC, Keller GR, Gridley JM, Leutgert JH, Mooney WD, Thybo H (1997) Crustal structure along the west flank of the Cascades, western Washington. J Geophys Res 102:17857–17873
Miura S, Sato T, Hasegawa A, Suwa Y, Tachibana K, Yui S (2004) Strain concentration zone along the volcanic front derived by GPS observations in NE Japan arc. Earth Planets Space 56:1347–1355
Montone P, Mariucci MT, Pierdominici S (2012) The Italian present-day stress map. Geophys J Int 189:705–716
Moore DE, Hickman S, Lockner DA, Dobson PF (2001) Hydrothermal minerals and microstructures in the Silangkitang geothermal field along the Great Sumatran fault zone, Sumatra, Indonesia. Geol Soc Am Bull 113:1179–1192
Mora D, Tassara A (2019) Upper crustal decompression due to deglaciation-induced flexural unbending and its role on post-glacial volcanism at the Southern Andes. Geophys J Int 216:1549–1559
Mount VS, Suppe J (1992) Present-Day stress orientations adjacent to Active Strike-Slip Faults: California and Sumatra. J Geophys Res 97:11995–12013
Mouslopoulou V, Hristopulos DT, Nicol A, Walsh JJ, Bannister S (2013) The importance of microearthquakes in crustal extension of an active rift: a case study from New Zealand. J Geophys Res 118:1556–1568
Nairn IA, Cole JW (1981) Basalt dikes in the 1886 Tarawera rift. NZ J Geol Geophys 24:585–592
Nakajima J, Hasegawa A (2004) Shear-wave polarization anisotropy and subduction-induced flow in the mantle wedge of northeastern Japan. Earth Planet Sci Lett 225:365–377
Natawidjaja DH, Triyoso W (2007) The Sumatran fault zone—from source to hazard. J Earthquake Tsunami 1:21–47
Okada T, Umino N, Hasegawa A (2010) Deep structure of the Ou mountain range strain concentration zone and the focal area of the 2008 Iwate-Miyagi Nairiku earthquake, NE Japan—seismogenesis related with magma and crustal fluid. Earth Planets Space 62:347–352
Oncken O, Hindle D, Kley J, Elger K, Victor P, Schemmann K (2006) Deformation of the Central Andean Upper Plate System—Facts, fiction, and constraints for plateau models. In: Oncken O, Chong G, Franz G, Giese P, Götze H-J, Ramos VA et al (eds) The andes—active subduction orogeny. Springer, Berlin, pp 3–27
Ozawa S, Nishimura T, Suito H, Kobayashi T, Tobita M, Imakiire T (2011) Coseismic and postseismic slip of the 2011 magnitude-9 Tohoku-Oki earthquake. Nature 475:373–376
Parsons T, Thompson GA, Smith RP (1998) More than one way to stretch: a tectonic model for extension along the plume track of the Yellowstone hotspot and adjacent Basin and Range Province. Tectonics 17:221–234
Passaro S, Tamburrini S, Vallefuoco M, Tassi F, Vaselli O, Giannini L (2016) Seafloor doming driven by degassing processes unveils sprouting volcanism in coastal areas. Sci Rep 6:22448. https://doi.org/10.1038/srep22448
Patacca E, Sartori R, Scandone P (1990) Tyrrhenian basin and apenninic arcs: kinematic relations since late Tortonian times. Mem Soc Geol It 45:425–451
Peccerillo A (2017) Cenozoic volcanism in the tyrrhenian sea region. In: Advances in Volcanology Springer International Publishing, AG, 415 pp
Pesicek JD, Thurber CH, Widiyantoro S, Engdahl ER, DeShon HR (2008) Complex slab subduction beneath northern Sumatra. Geophys Res Lett 35:L20303. https://doi.org/10.1029/2008GL035262

Petrinovic IA, Riller U, Alvarado G, Brod JA, Arnosio M (2006) Bimodal volcanism in a tectonic transfer zone: evidence for tectonically controlled magmatism in the southern Central Andes, NW Argentina. J Volcanol Geoth Res 152:240–252

Pezzopane SK, Weldon RJ (1993) Tectonic role of active faulting on central Oregon. Tectonics 12:1140–1169

Pitcher BW, Kent AJR (2019) Statistics and segmentation: using big data to assess cascades arc compositional variability. Geochim Cosmochim Acta 265:443–467

Pitcher BW, Kent AJR, Grunder AL, Duncan RA (2017) Frequency and volumes of ignimbrite eruptions following the Late Neogene initiation of the Central Oregon High Cascades. J Volcanol Geoth Res 339:1–22

Poland MP, Lisowski M, Dzurisin D, Kramer R, McLay M, Pauk B (2017) Volcano geodesy in the Cascade Arc, USA. Bull Volcanol 79:59

Pollitz FF, McCrory PM, Wilson D, Svarc J, Puskas C, Smith RB (2010) Viscoelastic-cycle model of interseismic deformation in the northwestern United States. Geophys J Int 181:665–696

Pollitz FF (1986) Pliocene change in Pacific-plate motion. Nature 320:738–741

Prawirodirdjo L, Bock Y, Genrich JF (2000) One century of tectonic deformation along the Sumatran fault from triangulation and Global Positioning System surveys. J Geophys Res 105:28343–28361

Priest GR (1990) Volcanic and tectonic evolution of the cascade volcanic arc, central oregon. J Geophys Res 95:19583–19599

Pritchard ME, Jay JA, Aron F, Henderson ST, Lara LE (2013) Subsidence at southern Andes volcanoes induced by the 2010 Maule, Chile earthquake. Nat Geosci 6:632–636

Pritchard ME, de Silva SL, Michelfelder G, Zandt G, McNutt SR, Gottsmann J et al (2018) Synthesis: PLUTONS: investigating the relationship between pluton growth and volcanism in the Central Andes. Geosphere 14:954–982

Kamesh Raju KA, Ray D, Mudholkar A, Murty GPS, Gahalut VK, Samudrala K et al (2012) Tectonic and volcanic implications of a cratered seamount off Nicobar Island, Andaman Sea. J Asian Earth Sci 56:42–53

Reath K, Pritchard ME, Moruzzi S, Alcott A, Coppola D, Pieri D (2019) The AVTOD (ASTER Volcanic Thermal Output Database) Latin America archive. J Volcanol Geoth Res 376:62–74

Riller U, Petrinovic IA, Ramelow J, Grekowiak J, Strecker M, Onken O (2001) Late Cenozoic tectonism, caldera and plateau formation in the central Andes. Earth Planet Sci Lett 188:299–311

Rosenau M, Melnick D, Echtler H (2006) Kinematic constraints on intra-arc shear and strain partitioning in the southern Andes between 38°S and 42°S latitude. Tectonics 25:4013. https://doi.org/10.1029/2005TC001943

Rosenbaum G, Gasparon M, Lucente FP, Peccerillo A, Miller MS (2008) Kinematics of slab tear faults during subduction segmentation and implications for Italian magmatism. Tectonics 27:TC2008. https://doi.org/10.1029/2007TC002143

Rosi M, Sbrana A (1987) Phlegraean fields. CNR Quaderni Ricerca Scientifica Roma 114:167 pp

Rowland JV, Wilson CJN, Gravley DM (2010) Spatial and temporal variations in magma-assisted rifting, Taupo Volcanic Zone, New Zealand. J Volcanol Geoth Res 190:89–108

Royden L, Patacca E, Scandone P (1987) Segmentation and configuration of subducted lithosphere in Italy: an important control on thrust-belt and foredeep-basin evolution. Geology 15:714–717

Ruch J, Vezzoli L, De Rosa R, Di Lorenzo R, Acocella V (2016) Magmatic control along a strike-slip volcanic arc: the central Aeolian arc (Italy). Tectonics 35:407–424

Santacroce R (1987) Somma Vesuvius. CNR Quaderni Ricerca Scientifica Roma, 251 pp

Sato H (1994) The relationship between late Cenozoic tectonic events and stress field and basin development in northeast Japan. J Geophys Res 99:22261–22274

Savelli C, Ligi M (2017) An updated reconstruction of basaltic crust emplacement in Tyrrhenian sea, Italy. Sci Rep 7:18024. https://doi.org/10.1038/s41598-017-17625-2

Schilling FR, Trumbull RB, Brasse H, Haberland C, Asch G, Bruhn G et al (2006) Partial melting in the Central Andean crust: a review of geophysical, petrophysical and petrologic evidence. In: Oncken O, Chong G, Franz G, Giese P, Götze H-J, Ramos VA et al (eds) The Andes—active subduction orogeny. Springer, Berlin, pp 459–474

Schmidt ME, Grunder AL, Rowe MC (2008) Segmentation of the Cascade Arc as indicated by Sr and Nd isotopic variation among diverse primitive basalts. Earth Planet Sci Lett 266:166–181

Schurr B, Asch G, Rietbrock A, Kind R, Pardo M, Heit B et al (1999) Seismicity and average velocities beneath the Argentine Puna plateau. Geophys Res Lett 26:3025–3028

Schurr B, Asch G, Rietbrock A, Trumbull RB, Haberland C (2003) Complex patterns of fluid and melt transport in the central Andean subduction zone revealed by attenuation tomography. Earth Planet Sci Lett 215:105–119

Schurr B, Rietbrock A, Asch G, Kind R, Oncken O (2006) Evidence for lithospheric detachment in the Central Andes from local earthquake tomography. Tectonophysics 415:203–223

Seebeck H, Nicol A (2009) Dike intrusion and displacement accumulation at the intersection of the Okataina Volcanic centre and Paeroa Fault zone, Taupo Rift, New Zealand. Tectonophysics 475:575–585

Sepúlveda F, Lahsen A, Bonvalot S, Cembrano J, Alvarado A, Letelier P (2005) Morpho-structural evolution of the Cordón Caulle geothermal region, Southern Volcanic Zone, Chile: insights from gravity and $^{40}Ar/^{39}Ar$ dating. J Volcanol Geoth Res 148:165–189

Serpelloni E, Anzidei M, Baldi P, Casula G, Galvani A (2005) Crustal velocity and strain-rate fields in Italy and surrounding regions: new results from the analysis of permanent and non-permanent GPS networks. Geophys J Int 161:861–880

Shearer P, Burgmann R (2010) Lessons learned from the 2004 Sumatra-Andaman megathrust rupture. Ann Rev Earth Planet Sci 38:103–131

Sieh K, Natawidjaja D (2000) Neotectonics of the Sumatran fault, Indonesia. J Geophys Res 105:28295–28326

Sielfeld G, Cembrano J, Lara L (2017) Transtension driving volcano-edifice anatomy: insights from andean transverse-to-the-orogen tectonic domains. Quatern Int 438:33–49

Sielfeld G, Lange D, Cembrano J (2019) Intra-arc crustal seismicity: seismotectonic implications for the southern Andes volcanic zone, Chile. Tectonics 38:552–578

Singer BS, Jicha BR, Harper MA, Naranjo JA, Lara LE, Moreno-Roa H (2008) Eruptive history, geochronology and magmatic evolution of the Puyehue-Cordon Caulle volcanic complex, Chile. Geol Soc Am Bull 120:599–618

Spinks K, Acocella V, Cole J, Bassett K (2005) Structural control of volcanism and caldera development in the transtensional Taupo Volcanic Zone, New Zealand. J Volcanol Geoth Res 144:7–22

Stankiewicz J, Ryberg T, Haberland C, Fauzi ND (2010) Lake Toba volcano magma chamber imaged by ambient seismic noise tomography. Geophys Res Lett 37:L17306. https://doi.org/10.1029/2010GL044211

Stern TA, Stratford WR, Salmon ML (2006) Subduction evolution and mantle dynamics at a continental margin: Central North Island, New Zealand. Rev Geophys 44:RG4002

Stern CR (2004) Active Andean volcanism: its geologic and tectonic setting. Revista Geológica De Chile 31:161–206

Subarya C, Chlieh M, Prawirodirdjo L, Avouac JP, Bock Y, Sieh K et al (2006) Plate boundary deformation associated with the great Sumatra-Andaman earthquake. Nature 440:46–51

Takada Y, Fukushima Y (2013) Volcanic subsidence triggered by the 2011 Tohoku earthquake in Japan. Nat Geosci 6:637–641

Tamura Y, Tatsumi Y, Zhao D, Kido Y, Shukuno H (2002) Hot fingers in the mantle wedge: new insights into magma genesis in subduction zones. Earth Planet Sci Lett 197:105–116

Tassara A, Yanez G (2003) Relationship between elastic thickness and the tectonic segmentation of the Andean margin. Rev Geol Chile 30:159–186

Tibaldi A, Corazzato C, Rovida A (2009) Miocene-Quaternary structural evolution of the Uyuni-Atacama region, Andes of Chile and Bolivia. Tectonophysics 471:114–135

Tibaldi A, Bonali FL, Corazzato C (2017) Structural control on volcanoes and magma paths from local- to orogen-scale: the central Andes case. Tectonophysics 699:16–41

Toda S, Stein RS, Sagiya T (2002) Evidence from the AD 2000 Izu islands earthquake swarm that stressing rate governs seismicity. Nature 419:58–61

Trumbull RB, Riller U, Oncken O, Scheuber E, Munier K, Hongn F (2006) The time-space distribution of Cenozoic volcanism in the south-central Andes: a new data compilation and some tectonic implications. In: Oncken O, Chong G, Franz G, Giese P, Götze H-J, Ramos VA et al (eds) The Andes—active subduction orogeny. Springer, Berlin, pp 29–43

Vezzoli L (1988) Island of Ischia. CNR Quaderni Ricerca Scientifica Roma 114, 133 pp

Villamor P, Berryman K (2001) A late Quaternary extension rate in the Taupo Volcanic Zone, New Zealand, derived from fault slip data. NZ J Geol Geophys 44:243–269

Villamor P, Van Dissen R, Alloway BV, Palmer AS, Litchfield N (2007) The Rangipo fault, Taupo rift, New Zealand: an example of temporal slip-rate and single event displacement variability in a volcanic environment. Geol Soc Am Bull 119:529–547

Villamor P, Berryman KR, Nairn IA, Wilson K, Litchfield N, Ries W (2011) Associations between volcanic eruptions from Okataina volcanic center and surface rupture of nearby active faults, Taupo rift, New Zealand: insights into the nature of volcano-tectonic interactions. Geol Soc Am Bull 123:1383–1405

Villamor P, Berryman KR, Ellis SM, Schreurs G, Wallace LM, Leonard GS et al (2017) Rapid evolution of subduction-related continental intraarc rifts: the Taupo Rift, New Zealand. Tectonics 36:2250–2272

Volker D, Kutterolf S, Wehrmann H (2011) Comparative mass balance of volcanic edifice at the southern volcanic zone of the Andes between 33° and 46°S. J Volcanol Geoth Res 205:114–129

Wada I, He J, Hasegawa A, Nakajima J (2015) Mantle wedge flow pattern and thermal structure in Northeast Japan: Effects of oblique subduction and 3-D slab geometry. Earth Planet Sc Lett 426:76–88

Waldien TS, Meigs AJ, Madin IP (2019) Active dextral strike-slip faulting records termination of the Walker Lane belt at the southern Cascade arc in the Klamath graben, Oregon, USA. Geosphere 15:882–900

Wallace LM, Beavan J, McCaffrey R, Darby D (2004) Subduction zone coupling and tectonic block rotations in the North Island, New Zealand. J Geophys Res 109: B12406. https://doi.org/10.1029/2004JB003241

Walter TR, Amelung F (2007) Volcanic eruptions following M $\geq$ 9 megathrust earthquakes: implications for the Sumatra-Andaman volcanoes. Geology 35:539–542

Ward KM, Zandt G, Beck SL, Christensen DH, McFarlin H (2014) Seismic imaging of the magmatic underpinnings beneath the Altiplano-Puna volcanic complex from the joint inversion of surface wave dispersion and receiver functions. Earth Planet Sci Lett 404:43–53

Watt SFL, Pyle DM, Mather TA (2009) The influence of great earthquakes on volcanic eruption rate along the Chilean subduction zone. Earth Planet Sci Lett 277:399–407

Weaver CS, Grant WC, Shemeta JE (1987) Local crustal extension at Mount St. Helens, Washington. J Geophys Res 92:10170–10178

Weller O, Lange D, Tilmann F, Natawidjaja D, Rietbrock A, Collings R et al (2012) The structure of the Sumatran Fault revealed by local seismicity. Geophys Res Lett 39:L01306. https://doi.org/10.1029/2011GL050440

Wells RE (1990) Paleomagnetic rotations and the Cenozoic Tectonics of the Cascade Arc, Washington, Oregon, and California. J Geophys Res 95:19409–19417

Wells RE, McCaffrey R (2013) Steady rotation of the Cascade Arc. Geology 41:1027–1030

Widiwijayanti C, Deverchere J, Louat R, Sebrier M, Harjono H, Diament M et al (1996) Aftershock sequence of the 1994, Mw 6.8, Liwa earthquake (Indonesia): seismic rupture process in a volcanic arc. Geophys Res Lett 23:3051–3054

Wilson CJN, Houghton BF, McWilliams MO, Lanphere MA, Weaver SD, Briggs RM (1995) Volcanic and structural evolution of Taupo Volcanic Zone, New Zealand: a review. J Volcanol Geoth Res 68:1–28

Wilson CJN (1996) Taupo's atypical arc. Nature 379:27–28

Wortel MJR, Spakman W (2000) Subduction and Slab Detachment in the Mediterranean-Carpathian Region. Science 290:1910–1917

Yoshida T, Kimura J, Yamada R, Acocella V, Sato H, Zhao D et al (2013) Evolution of the Late Cenozoic Magmatism and the crust-mantle structure in the NE Japan Arc. Geol Soc London Spec Publ 385. https://doi.org/10.1144/SP385.15

Yoshida T (2001) The evolution of arc magmatism in the NE Honshu arc, Japan. Tohoku Geophys J 36:131–249

Zellmer GF, Chen K-X, Gung Y, Kuo B-Y, Yoshida T (2019) Magma transfer processes in the NE Japan Arc: insights from crustal ambient noise tomography combined with volcanic eruption records. Front Earth Sci 7:40. https://doi.org/10.3389/feart.2019.00040